Modeling the Transition Region

Bart A. Singer
High Technology Corporation Research Scientist
Mail Stop 156, NASA Langley Research Center
Hampton, VA 23681

Contents

1 Introduction **5**

2 The Domain of Dependence–Flow Features That Affect Transition **15**

2.1 Pressure Gradients 15
2.2 Compressibility 16
2.3 Free-Stream Disturbances 16
2.4 Surface Roughness 16
2.5 Streamline Curvature 17
2.6 Three-Dimensional Mean Flows 17
2.7 Unsteady Mean Flows 17
2.8 Surface Heating and Cooling 18
2.9 Mass Injection or Suction 18
2.10 Separated Flows 19

3 Model Classifications **20**

3.1 General 20
3.2 Turbulence Models 21
3.2.1 Direct Numerical Simulation and Large-Eddy Simulation 21
3.2.2 Statistical Turbulence Models 22
3.2.3 Integral Methods 23
3.3 Transition-Region Models 23
3.3.1 Linear-Combination Models 23
3.3.2 Algebraic Models 24
3.3.3 Differential Models 24

4 Fully Turbulent Flow Models **25**
4.1 Basic Equations 25
4.2 Eddy-Viscosity Turbulence Models 27
4.2.1 Algebraic or Zero-Equation Models 28
4.2.2 One-Equation Models 29
4.2.3 Two-Equation Models 34
4.3 Reynolds Stress Transport Turbulence Models 41
4.4 Large-Eddy Simulation 45

5 Transition-Region Models **48**
5.1 Linear-Combination Transition-Region Models 48
5.2 Algebraic Transition-Region Models 50
5.3 Differential Transition-Region Models 52
5.3.1 The Two-Layer $k-\epsilon$ Model 55
5.3.2 Schmidt and Patankar $k-\epsilon$ Model 56
5.3.3 Wilcox $k-\omega$ Model 57
5.3.4 LES Models for Transition 58
5.3.5 Questions Regarding Model Initiation 59
5.4 Unconventional Approaches 60

6 Evaluation of Transition Models **63**
6.1 A Systematic Method 63
6.2 The T3 Test-Case Project 66
6.3 All Data Are NOT Equal–Some Notes on the Use of Experimental Data 69

7 Summary and Author's Views **71**

Statement of Purpose

My goal is to introduce you to a spectrum of approaches used to model the transition region, make you aware of the challenges in such a task, and provide some tools to help you make decisions as to the most appropriate way to address your individual problems.

Opinions of the Experts

We will initiate the learning process with a quick look at how various experts of transition and turbulence modeling responded to my requests for their personal ideas about the future of transition-region modeling. I have edited their responses (as indicated by the [...]'s) only to the extent necessary to preserve anonymity and clarify acronyms. I hope that these notes will provide you with the knowledge to intelligently evaluate these opinions and to confidently reach your own conclusions.

"For the next couple of years I see that $k - \epsilon$ models [...] will be used for practical calculations. Perhaps slowly Reynolds stress models will take over, but very little has so far been done with these in the area of transition modeling. I believe that the future belongs to large-eddy simulations, and I expect that in 5 to 10 years' time transition calculations will be done by such simulations also for practical purposes."

"For engineering prediction procedures in the gas-turbine industry (i.e., for flows with high free-stream turbulence intensity) I recommend to put more efforts into second-moment closure (Reynolds stress modeling). For aerodynamic applications (i.e., low free-stream turbulence intensities) I am afraid one is left with even more empirical transition correlations."

"I would expect Reynolds stress approaches to be the simplest level that can usefully tackle transition on aircraft in subsonic or hypersonic flows (though current schemes are almost certainly inadequate for the latter task). They will need some help in getting started – possibly some kind of library built up from separate DNS [direct numerical simulation] studies. On gas-turbine blades, two-equation schemes may suffice, particularly if one makes use of the available strain and vorticity invariants to render the scheme more appropriately sensitive to curvature and irrotational deformations of the mean velocity field."

"Low-Re RST [Reynolds stress transport] modeling will be vital for real predictions of transition – possibly linked to intermittency or other treatments for $Tu < 1\%$ – at least at subsonic conditions in both external and internal environments. Simpler models (i.e., $k - \epsilon$) with additional refinements may be needed for unstructured Navier-Stokes solutions with adaptive meshes for complex geometries. Yet simpler derivative models – perhaps based on Johnson and King–type nonequilibrium approaches and Grundmann et al. ideas may be the limit for real (hypersonic) aircraft computations."

Chapter 1

Introduction

The calculation of engineering flows undergoing laminar-turbulent transition presents special problems. Mean-flow quantities obey neither the fully laminar nor the fully turbulent correlations. In addition, local maxima in skin friction, wall temperature, and heat transfer often occur near the end of the transition region. Traditionally, modeling this region has been important for the design of turbine blades, where the transition region is long in relation to the chord length of the blade. More recently, the need for better transition-region models has been recognized by designers of hypersonic vehicles where the high Mach number, the low Reynolds number, and the low-disturbance flight environment emphasize the importance of the transition region. Needless to say, a model that might work well for the transitional flows typically found in gas turbines will not necessarily work well for the external surface of a hypersonic vehicle. In Chapter 2, some of the important flow features that control the transition region will be discussed. In Chapter 3, different approaches to the modeling problem will be summarized and cataloged. Fully turbulent flow models will be discussed in detail in Chapter 4; models specifically designed for transitional flow, in Chapter 5; and the evaluation of models, in Chapter 6. Finally, in Chapter 7, the major points will be summarized and then I will take the opportunity to express my own opinions.

Nomenclature

A	length scale used in near-wall exponential damping
A_μ	constant for damping turbulent transport length scale
A^+	normalized length scale used in near-wall exponential damping
a	$= -\overline{u'v'}/(2k)$, structure coefficient
a_{ij}	$= (\overline{u_i'u_j'} - 2/3\delta_{ij}k)/k$, anisotropic part of Reynolds stress tensor
a_1	coefficient used in setting initial dissipation-rate profile
B_1, B_2	empirical parameters
C_f	$= \mu \frac{dU}{dy}\|_w/(\frac{1}{2}\rho U^2)$, skin-friction coefficient
C_{ijk}	turbulent-stress diffusion correlation
c_l	length-scale coefficient
c_p	specific heat at constant pressure
c_s	diffusion coefficient for turbulent stress
$c_\epsilon, c_{\epsilon 1}, c_{\epsilon 2}$	parameters used in modeling of dissipation
$c_\epsilon, c_{\epsilon 1}, c_{\epsilon 2}$	parameters used in modeling of dissipation
c_μ	coefficient in eddy viscosity
c_1	coefficient in production term in dissipation-rate equation
c_2	coefficient in destruction term in dissipation-rate equation

c_1, c_2, c_1^w, c_2^w	parameters used in modeling of Π_{ij}
D	material derivative
$\mathcal{D}_\epsilon$	turbulent diffusion of ϵ
E	empirical source term used in the equation for ϵ
F	fudge factor used to make a tensor contract correctly
f_s	low Reynolds number damping function
f_ϵ	low Reynolds number damping function of dissipation
f_μ	low Reynolds number damping function in eddy viscosity
f_1	low Reynolds number function in production term in dissipation-rate equation
f_2	low Reynolds number function in destruction term in dissipation-rate equation
g_i	body force
G	filter function for large-eddy simulation
h	specific enthalpy
k	$= \frac{1}{2}\overline{u_i' u_i'}$, turbulent kinetic energy per unit mass
k_{th}	thermal conductivity
L	length of transition region
L_{t2}	$= \frac{dU_e}{dx}\theta_{lam}^2/\nu$, pressure-gradient parameter at x_{t2}

$\mathcal{L}_{ij}$	smallest resolved stresses in large-eddy simulation
l_ϵ	turbulent dissipation length scale
l_μ	turbulent transport length scale
l_0, l_1, l_2	length scales for zero-equation, one-equation, and two-equation models
M	Mach number
M_{ij}	subgrid-scale model for anisotropic part of T_{ij}
m_{ij}	subgrid-scale model for anisotropic part of τ_{ij}
N	exponent in e^N transition-prediction method
N_0	nominal nondimensional spot-formation rate
N_2	adjusted nondimensional spot-formation rate
n_j	wall-normal component of unit vector in j direction
P_k	production of turbulent kinetic energy
P_{ij}	stress production rate tensor
$\mathcal{P}_\epsilon$	production of turbulent dissipation
p	pressure
p'	fluctuating pressure
p'_T	fluctuating total pressure
p^+	$= -\mu_e U_e \frac{dU_e}{dx}/(\rho_e u_\tau^3)$, nondimensional pressure gradient

q	$= \frac{1}{2}\rho U^2$, dynamic pressure
$\dot{q}$	heat flux
R_T	$= k^2/(\epsilon\nu)$, turbulent Reynolds number
R_k, R_w, R_β	constants in low Reynolds number version of $k-\omega$ model
R_y	$= yk^{1/2}/\nu$, turbulent Reynolds number based on y
Re	Reynolds number based on streamwise distance
Re_L	Reynolds number based on length scale L
Re_{T0}	Reynolds number at end of transition
Re_{t0}	Reynolds number at start of transition
Re_{xs}	Reynolds number based on x location of the start of transition
Re_θ	Reynolds number based on momentum thickness
$Re_{\theta s}$	Reynolds number based on momentum thickness at the start of transition
Re_1	unit Reynolds number
r	$= (T_{aw}-T_e)/(T_T-T_e)$, recovery factor
S	$= \sqrt{2S_{ij}S_{ij}}$
S_{ij}	$= \frac{1}{2}(\frac{\partial u_i}{\partial x_j}+\frac{\partial u_j}{\partial x_i})$, strain rate
St	$= \dot{q}/\left[\rho c_p(T_w-T_e)\right]$, Stanton number
T	temperature

T_T	total temperature
T_{ij}	subgrid-scale stress on test filter
Tu	$= \sqrt{u_i' u_i'/3}/U_e \times 100$, turbulence intensity (in percent)
t	time
U	mean streamwise velocity
u_i	velocity in the ith direction
u_τ	$= \sqrt{\mu \frac{dU}{dy}\|_w/\rho}$, friction velocity
u'	velocity fluctuation in the streamwise direction
u_i'	velocity fluctuation in the ith direction
v'	velocity fluctuation in the wall-normal direction
$\mathbf{x}$	coordinate vector
x_{T0}	streamwise position at end of transition
x_i	coordinate in the ith direction
x_{t0}	streamwise position at start of transition
y	$= x_2$, wall-normal coordinate
y^+	$= y u_\tau/\nu$, wall-normal coordinate normalized by viscous scales
α	angle of pitch
α, α^*	functions used in $k-\omega$ model

β	angle of yaw
β, β^*	functions used in $k-\omega$ model
γ	turbulent intermittency
γ_t	transition function
Δ	filter width associated with subgrid-scale models
δ_{ij}	$= 1$ if $i = j$, 0 otherwise
δ^*	displacement thickness
ϵ	turbulent energy-dissipation rate
$\tilde{\epsilon}$	modified dissipation rate
ϵ_{ij}	dissipation-rate tensor
θ	momentum thickness
κ	von Karman constant (≈ 0.41)
λ	distance between points where $\gamma = 0.25$ and $\gamma = 0.75$
λ_θ	$= \frac{dU_e}{dx}\theta^2/\nu$, pressure-gradient parameter
μ	dynamic-viscosity coefficient
μ_{eff}	effective dynamic-viscosity coefficient
μ_t	turbulent dynamic-viscosity coefficient
ν	$= \mu/\rho$, kinematic-viscosity coefficient

ν_t	$= \mu_t/\rho$, turbulent kinematic-viscosity coefficient
Π_{ij}	pressure-strain correlation tensor
$\Pi_{ij1}, \Pi_{ij2}, \Pi_{ij1}^w, \Pi_{ij2}^w$	parts of the modeled pressure-strain correlation
ρ	density
σ_k	Prandtl number for diffusion of k
σ_ϵ	Prandtl number for diffusion of ϵ
σ_ω	Prandtl number for diffusion of ω
τ	$= 1/\omega$, turbulent time scale
τ_{ij}	$= \overline{u_i u_j} - \bar{u}_i \bar{u}_j$, subgrid-scale stress
χ_1	correlating parameter for ONERA/CERT transition model
Φ	viscous-dissipation function
Φ_ϵ	turbulent destruction of dissipation in ϵ equation
ω	$= \epsilon/(\beta^* k)$, a turbulence quantity proportional to the dissipation rate per unit kinetic energy
$()'$	deviation from Reynolds average
$()''$	deviation from mass-weighted average
$\widetilde{()}$	mass-averaged quantity or LES test-filtered quantity
$\overline{()}$	Reynolds-averaged quantity or LES grid-filtered quantity

Subscripts:

aw	adiabatic wall quantity
D	a damped quantity, usually because of wall proximity
e	boundary-layer edge quantity
i, j, k, l, m	tensor indices (summation over repeated indices is implied)
lam	a laminar-flow quantity
max	maximum
sgs	subgrid-scale quantity
T	total
t	turbulent
$t0$	value at start of turbulent boundary layer
$t2$	value at point of "subtransition"
w	wall quantity
∞	free-stream quantity (upstream of shock if applicable)

Acronyms:

ERCOFTAC	Europeon Research Community on Flow Turbulence and Combustion
DNS	direct numerical simulation
LES	large-eddy simulation

RANS	Reynolds-averaged Navier-Stokes
RST	Reynolds stress transport
RNG	renormalization group
SGS	subgrid scale
SIG	special interest group
TS	Tollmien-Schlichting

Chapter 2

The Domain of Dependence–Flow Features That Affect Transition

The location and length of the transition region is sensitive to a number of different flow features. Although the following summary is by no means complete, it describes the sort of phenomena that may require consideration in modeling the transition region.

2.1 Pressure Gradients

Adverse and favorable pressure gradients affect both the onset of transition and the length of the transition region. Large, favorable pressure gradients may even relaminarize an already turbulent flow [1]. Favorable pressure gradients in a laminar flow lead to a delayed onset of transition and a more extensive transition region (see [2]). The results of linear stability theory can explain the delayed onset; Narasimha, Subramanian, and Badri Narayanan [3] suggest that these results can also explain the greater extent of the transition zone. Transition in attached boundary layers with adverse pressure gradients starts earlier, extends for a shorter distance, and is more two dimensional than transition in zero-pressure-gradient flows [4]. The formation of a laminar separation bubble in the flow raises the possibility of a free-shear layer instability that leads to transition.

2.2 Compressibility

Compressibility effects are important in several ways. The Mach number influences the mean flow of a boundary layer and the nature of the stability equations. At Mach numbers greater than approximately 2, an inviscid instability can have a significant effect during transition. This instability has its critical layer far from the wall; hence, the typical sequence of events observed for incompressible flows may not occur. In addition, as the fluctuation Mach number increases above 0.3, the resulting turbulence [5] becomes significantly different from that of the subsonic case.

2.3 Free-Stream Disturbances

Free-stream turbulence (vorticity), entropy (temperature), and acoustic (pressure) disturbances are present in all flows to varying extents. In subsonic wind tunnels with turbulence generating grids, most of the disturbance is vortical (i.e., turbulent) in nature. In quiet subsonic ($Tu < 0.1\%$) and in transonic and supersonic wind tunnels, most of the free-stream disturbances are acoustic [6]. The type of free-stream disturbances in practical applications is likely to be quite dependent on the particular application. Bushnell [7] notes that subsonic powered aircraft are highly susceptible to acoustic disturbances radiated from the engine and airframe, while particulates can be a source of vortical disturbances at altitudes up to 24 km. The turbine blades in a gas-turbine engine probably experience free-stream disturbances of all three types.

2.4 Surface Roughness

All surfaces have some degree of roughness. Joints and fasteners act as large, discrete roughness elements, while multiple scratches, insect debris, and material inhomogeneities all contribute to distributed roughness. The effects of the surface imperfections can vary dramatically [8] depending upon the characteristics of the roughness and the boundary layer at the location of the roughness. Large roughness elements can be a source of turbulence via a bypass mechanism. The bypass can occur right at the roughness element

or further downstream. The roughness can also act to enhance the primary instabilities or as a source of receptivity for these disturbances.

2.5 Streamline Curvature

The Görtler instability that develops in regions of concave wall curvature is fundamentally different from the usual viscous instabilities that initiate transition on flat plates [9]. Instead of streamwise traveling waves, the Görtler instability manifests itself as pairs of counterrotating vortices. These vortices distort the time-averaged, streamwise-velocity profile long before the flow can be considered turbulent. Important differences in the physics of the transition process are possible in this case.

2.6 Three-Dimensional Mean Flows

Three-dimensional boundary layers are subject to inviscid crossflow instabilities that result in both stationary and traveling vortices in the flow. These instabilities are generally important near the leading edges of swept wings and on bodies of revolution at angles of attack [10]. As with the Görtler vortices, the stationary vortices that are excited by the crossflow instability can lead to significant distortion of the time-averaged flow quantities upstream of where the flow would be considered turbulent.

2.7 Unsteady Mean Flows

Flows on compressor and turbine blades are subject to the periodic impingement of turbulent wakes shed from the upstream blade row. This impingement causes a turbulent "strip" to form across the span of the blade [1]. This strip of turbulence propagates downstream along the blade at a velocity less than that of the wake. Regions of wake-induced transition typically are separated by a region in which a nominally steady, normal transition takes place. Hence, multiple modes of transition can be present simultaneously on the same surface.

2.8 Surface Heating and Cooling

The effects of surface heating and cooling on laminar-turbulent transition are varied. For subsonic flows, the effects of heating and cooling are a consequence of the temperature dependence of viscosity and of the effect of viscosity on the mean flow profile [11]. Uniform heating in water boundary layers tends to stabilize the flow by decreasing the viscosity near the wall; in air, uniform heating tends to destabilize the flow. However, Masad and Nayfeh [12] show that a heating strip placed somewhat upstream of Branch I of the neutral stability curve can actually help stabilize an air boundary layer, presumably because the boundary layer that is downstream of the heating strip "sees" a relatively cooler wall.

The heating and cooling phenomena are further complicated for supersonic flow. In supersonic flow, cold walls (the typical situation for a reentry vehicle) generally stabilize the first instability mode (the mode that continues analytically from the most unstable subsonic mode). However, at Mach numbers somewhat greater than 2, cold walls destabilize the higher modes (Mack modes [13]). Preliminary results (Masad, personal communication) indicate that the heating strips that are upstream of the Branch I neutral curves produce trends that are similar to those obtained with global cooling for the respective modes.

For gas-turbine applications, the wall heating and cooling issue is probably of secondary importance. Experiments with high levels of free-stream turbulence ($Tu > 1.6\%$) in a subsonic flow indicate that wall cooling affects neither the location nor the length of transition [14].

2.9 Mass Injection or Suction

Mass injection is common on turbine blades, providing a protective blanket of relatively cool air around the blade. Fluid is typically injected near the nose of the blade, where strong, favorable pressure gradients are present. Mayle [1] reports that under these conditions, neither a laminar boundary layer nor a truly turbulent boundary layer exists, except perhaps much further downstream. In the presence of strong, favorable pressure gradients, the locally excited turbulent regions near the injection slots can relaminarize and undergo a normal transition further downstream.

The reverse process of wall suction is being used to help stabilize boundary layers in quiet flows and hence delay the onset of transition [15]. Optimization often involves the use of wall suction near Branch I of the neutral stability curve [12, 16, 17]. Suction typically is not applied in the transition region, so information is available only on the the onset of transition.

2.10 Separated Flows

Separated flows occur in adverse pressure gradients where the momentum of the fluid in the boundary layer is insufficient to overcome the pressure gradient. Boundary-layer separation is more common for laminar flows (which do not easily transport momentum across the boundary layer) than for turbulent flows (which do transport large amounts of momentum across the boundary layer). Typically, a region of laminar separated flow will undergo transition as a free-shear layer and then reattach as a turbulent flow. The length of the separation region can be either short or long; the short bubbles have only a local effect on flow, while the long bubbles interact extensively with the exterior flow and significantly modify the pressure distribution on the surface. Short bubbles may burst into long bubbles and possibly result in stall [1]. The limited data indicate that the transition lengths of both the long and short bubbles are essentially the same, with the difference in the bubble length mainly due to the length of the unstable laminar shear layer [1]. Some experts have theorized that the long bubbles undergo a primary instability while the short bubbles experience a bypass transition.

Chapter 3

Model Classifications

3.1 General

Models for transitional flows can be categorized in a variety of ways (e.g., by the numerical technique, by the type of turbulence model, or by the kind of transitional flow modifications). Because the success or failure of any model for the transitional flow regime is strongly coupled to the scheme used to calculate the incipient turbulent flow, a classification matrix can help distinguish between aspects of the model that are related to the turbulent flow calculation method and those aspects that are specific to the transition region. In table 3.1, approaches for calculating turbulent flows are listed in the left column. For direct numerical simulation (DNS), all relevant scales of motion are numerically resolved; the only modeling involved is that associated with the derivation of the Navier-Stokes equations and the boundary conditions used. In large-eddy simulation (LES), the large scales of motion are computed and the small scales are modeled. Four types of transport-equation models are listed, followed by integral methods. The higher order turbulence models appear near the top of the matrix; the lower order models are near the bottom. The other columns indicate the type of transition-region model as classified by Dey and Narasimha [18]. An x in the column indicates that a particular category of transition-region model is compatible with the corresponding turbulence model.

In the remainder of this section, the general features of each class of turbulence and transition-region model will be discussed. Later sections will

	Linear combination	Algebraic	Differential
Direct numerical simulation	x		x
Large-eddy simulation	x	x	x
Reynolds stress transport	x	x	x
Two-equation transport	x	x	x
One-equation transport	x	x	x
Zero-equation transport	x	x	
Integral methods	x		

Table 3.1: Possible combinations of turbulence models (rows) with transition-region models (columns).

include more detail.

3.2 Turbulence Models

3.2.1 Direct Numerical Simulation and Large-Eddy Simulation

Both the DNS and LES approaches require enormous amounts of computing resources, so these approaches are usually used on a supercomputer. The DNS approach, which involves no explicit turbulence modeling, is entirely a research tool that enables scientists to better understand various aspects of the physics of turbulence and can be used to guide the development of turbulence models. In LES, the small scales of turbulence, which are assumed to be more universal in nature, are modeled; the large, energy-containing scales that are more flow specific are explicitly calculated. The models used for the small scales are called subgrid-scale (SGS) models. Unlike other types of turbulence models discussed below, the resultant equations for LES describe a fully time-dependent flow; the modeling only blurs the turbulent structures so that the small scales do not need to be calculated. A potential exists for the practical use of LES in the near future, although the high cost will restrict its use to cases where lower order models are not expected to give satisfactory results.

3.2.2 Statistical Turbulence Models

Presently, statistical turbulence models are the most widely used turbulence-modeling schemes. Flow quantities are decomposed into mean and fluctuating parts and then substituted into the equations of motion. These equations are averaged to produce a set of equations for the mean motion. Osborne Reynolds pioneered this approach [19] by temporally averaging the equations for incompressible flow; the resultant equations are known as the Reynolds-averaged Navier-Stokes (RANS) equations. These equations involve the mean flow quantities as well as correlations of the fluctuating quantities. The correlations appear in the equations of mean motion in the same way as the viscous stress terms appear; hence, these correlations are known as the Reynolds stresses. The various classes of models differ in how these correlations are approximated.

Reynolds stress transport (RST) models involve transport equations for each of the six independent Reynolds stress components. This class of models is the most complex of the statistical turbulence models, and the use of these models for engineering applications is not yet commonplace. However, because the Reynolds stresses can independently respond to various flow conditions, this class of models can potentially be applied to a large variety of flows. This potential generality motivates much of the current research on these models.

Eddy-viscosity models include a number of classes of models, all of which approximate the effect of the turbulence on the mean motion by modifying the coefficient of viscosity. The effective viscosity coefficient that is used in the computation of the flow field is the sum of the molecular viscosity μ and the turbulent viscosity μ_t. The different classes of eddy-viscosity models are distinguished by the number of additional differential equations that are solved to determine μ_t. Dimensional analysis suggests that μ_t is the product of the density, a velocity scale, and a length scale. The local mean density is almost always used, leaving the velocity and length scale still to be determined. Two-equation models solve differential equations to determine these two scales. One-equation models solve a differential equation for the velocity scale and use algebraic relations to determine the length scale. Zero-equation models use algebraic relations to determine both the velocity and length scales. More detail on all of these model classes will be given in Chapter 4.

3.2.3 Integral Methods

In integral methods, an ordinary differential equation is solved for the momentum thickness θ in terms of the skin-friction coefficient C_f, the displacement thickness δ^*, the boundary-layer edge velocity, and body curvature. For flows with heat transfer, another equation is required that involves the Stanton number St, the enthalpy thickness, the free-stream and wall temperatures, and the body geometry. Approximate relationships between the variables are substituted into the equations. The equations are integrated in the downstream direction. These methods are computationally quite efficient, but are accurate only for those flows in which the assumed relationships are appropriate. Of the 20 integral methods that competed in the 1968 Stanford Conference [20, 21], only four received an evaluation of "good" after they were tested for 16 different turbulent flows. In spite of their limited generality, integral methods provide good skin-friction and heat-transfer predictions for well-studied flows of engineering interest. See White [22] for more details.

3.3 Transition-Region Models

3.3.1 Linear-Combination Models

Linear-combination models are based on the assumption that the transitional flow is composed of intermittent spots of turbulence in an otherwise fully laminar flow. Under this assumption, the time-averaged flow field is a linear combination of the laminar flow and a fully turbulent flow that originates where transition starts. The relative amounts of laminar and turbulent flow in the linear combination are governed by the intermittency γ, which is defined as the fraction of time that the flow is turbulent. The most difficult aspect of this approach is the determination of an appropriate distribution for the intermittency. An important feature of this type of model is that it can be coupled with any method of calculating the laminar and turbulent flows. The basic assumption of the model (i.e., the coexistence of fully laminar and fully turbulent states) has been questioned by some investigators who claim that the transition region, at least in some flows, is more complicated than a simple mixture of laminar and turbulent flows.

3.3.2 Algebraic Models

Algebraic models are designed to be incorporated into turbulence models that use an eddy-viscosity assumption. They involve a modification of the effective viscosity so that

$$\mu_{\text{eff}} = \mu + \gamma_t \mu_t \tag{3.1}$$

where γ_t is a transition function equal to zero before the start of transition and equal to 1 at the conclusion of transition. Different models use various functions to represent γ_t. Some models have γ_t approximate the flow intermittency γ (see [23]); in other models [24] γ_t is greater than 1 in parts of the transition region and so cannot represent the true intermittency. The use of algebraic models is convenient because these models involve very minor modifications to existing eddy-viscosity models.

3.3.3 Differential Models

Differential models address the issue of transition in the fundamental differential equations. The transition phenomena are often addressed simultaneously with other low Reynolds number modifications used in many of the turbulence models that use transport equations.

Chapter 4

Fully Turbulent Flow Models

In this chapter models for fully turbulent flow will be discussed. The particular models have been chosen because either they clearly illustrate important points about a group of models or they have been incorporated into a transitional flow model that is discussed in the next chapter.

Standard Cartesian tensorial notation is used; repeated indices imply a summation. Tensor indices are restricted to the letters i, j, k, l, and m. All other subscripts clarify variable meanings. Where specific variable directions are needed, the subscript 1 indicates the streamwise direction; the subscript 2, the wall-normal direction; and the subscript 3, the spanwise direction.

4.1 Basic Equations

For a Newtonian fluid, when the Stokes hypothesis is assumed, the Navier-Stokes equations can be written

$$\frac{\partial(\rho u_i)}{\partial t} + \frac{\partial(\rho u_i u_j)}{\partial x_j} = \rho g_i - \frac{\partial p}{\partial x_i} + \frac{\partial}{\partial x_j}\left[\mu\left(\frac{\partial u_i}{\partial x_j} + \frac{\partial u_j}{\partial x_i}\right) - \frac{2}{3}\mu\delta_{ij}\frac{\partial u_k}{\partial x_k}\right] \quad (4.1)$$

subject to conservation of mass

$$\frac{D\rho}{Dt} + \rho\frac{\partial u_k}{\partial x_k} = 0 \quad (4.2)$$

and conservation of energy

$$\rho\frac{Dh}{Dt} = \frac{Dp}{Dt} + \frac{\partial}{\partial x_k}\left(k_{\text{th}}\frac{\partial T}{\partial x_k}\right) + \Phi \quad (4.3)$$

where u_i is the velocity; p is the pressure; g_i is a body force; μ is the coefficient of viscosity; δ_{ij} is the Kroneker-delta; h is the specific enthalpy; k_{th} is the thermal conductivity; and $\Phi = (\partial u_i/\partial x_j)\mu\left[\partial u_i/\partial x_j + \partial u_j/\partial x_i - 2/3\left(\delta_{ij}\partial u_l/\partial x_l\right)\right]$ is the viscous dissipation function. For the remainder of this work, the body force will be neglected, although it could be retained if it were important in a particular application.

There are two common ways to decompose the flow variables, depending upon whether the flow must be treated as compressible. For incompressible flow, the standard Reynolds decomposition is

$$f \equiv \bar{f} + f' \tag{4.4}$$

where f is the flow quantity, $\bar{f}$ is the average, and f' is the fluctuation. The average can be either a temporal average or an ensemble average. With Reynolds averaging, the average of a fluctuating quantity is zero; hence,

$$\overline{f'} = 0 \tag{4.5}$$

The other common way to decompose the flow field is through the use of mass-weighted averages such that

$$f \equiv \tilde{f} + f'' \tag{4.6}$$

where

$$\tilde{f} \equiv \frac{\overline{\rho f}}{\bar{\rho}} \tag{4.7}$$

Note that

$$\overline{\rho f''} = 0 \tag{4.8}$$

but that

$$\overline{f''} \neq 0 \tag{4.9}$$

To keep the presentation of the modeling concepts unencumbered by algebraic messiness, unless specifically stated otherwise, the models will be discussed in their incompressible, isenthalpic form. Hence, the Reynolds-averaged equations can be written as

$$\frac{\partial \bar{u}_k}{\partial x_k} = 0 \tag{4.10}$$

$$\frac{\partial(\rho\bar{u}_i)}{\partial t} + \frac{\partial(\rho\bar{u}_i\bar{u}_j)}{\partial x_j}$$
$$= -\frac{\partial\bar{p}}{\partial x_i} + \frac{\partial}{\partial x_j}\left[\mu\left(\frac{\partial\bar{u}_i}{\partial x_j} + \frac{\partial\bar{u}_j}{\partial x_i}\right) - \frac{2}{3}\mu\delta_{ij}\frac{\partial\bar{u}_k}{\partial x_k} - \rho\overline{u_i'u_j'}\right] \tag{4.11}$$

The Reynolds stress is easily identified as $-\rho\overline{u_i'u_j'}$. Especially with an incompressible flow, mass-specific quantities are commonly used; hence, the term "Reynolds stress tensor" is often used to refer to the velocity correlation $-\overline{u_i'u_j'}$. This convention is used in this report so that, for incompressible flow, the turbulent kinetic energy is defined as

$$k \equiv \frac{1}{2}\overline{u_i'u_i'} \tag{4.12}$$

and the true dissipation rate of k is

$$\nu\,\overline{\frac{\partial u_i'}{\partial x_j}\left(\frac{\partial u_i'}{\partial x_j} + \frac{\partial u_j'}{\partial x_i}\right)} \tag{4.13}$$

The symbol ϵ is often defined as

$$\epsilon \equiv \nu\,\overline{\frac{\partial u_i'}{\partial x_j}\frac{\partial u_i'}{\partial x_j}} \tag{4.14}$$

and the additional term associated with the dissipation rate $\nu\overline{(\partial u_i'/\partial x_j)\left(\partial u_j'/\partial x_i\right)}$ is combined with viscous work terms in the kinetic energy equation to form the kinetic energy diffusion term $\nu\,(\partial^2 k/\partial x_i\partial x_i)$, as is done here. Although ϵ is commonly called the turbulent dissipation, Hinze [25] points out that this is the true dissipation only in homogeneous turbulence. For compressible flows, the dissipation is considerably more complicated. The additional complexity will not be addressed in this paper.

With the above background information, some simple turbulence models will be examined.

4.2 Eddy-Viscosity Turbulence Models

In eddy-viscosity models, the Reynolds stress tensor is approximated as

$$-\overline{u_i'u_j'} = 2\frac{\mu_t}{\rho}\bar{S}_{ij} - \frac{2}{3}k\delta_{ij} \tag{4.15}$$

where

$$\bar{S}_{ij} = \frac{1}{2}\left(\frac{\partial \bar{u}_i}{\partial x_j} + \frac{\partial \bar{u}_j}{\partial x_i}\right) \tag{4.16}$$

is the mean-flow strain rate and the last term on the right is needed for consistency with the definition of k.

4.2.1 Algebraic or Zero-Equation Models

In zero-equation turbulence models, an algebraic relation is used to determine the eddy viscosity. A mixing-length hypothesis suggests that the eddy viscosity take a form like:

$$\frac{\mu_t}{\bar{\rho}} = \nu_t = l_0^2 \left(\bar{S}_{ij}\bar{S}_{ij}\right)^{\frac{1}{2}} \tag{4.17}$$

where l_0 is a length scale obtained from an algebraic formula. The length scale represents the distance traveled by a hypothetical lump of fluid before that lump transfers its momentum to another lump of fluid. This level of modeling implies that the mean motion is unaffected by the turbulence intensity k. Two common zero-equation models are the models of Cebeci and Smith [26] and Baldwin and Lomax [27]. The Cebeci-Smith model generally works well in subsonic, equilibrium turbulent boundary layers. Many modifications to the model have extended the useful range of the model to a large variety of flows. The Baldwin-Lomax model was specifically designed to handle transonic and supersonic separated flows over airfoils. Both are two-layer models. In the Baldwin-Lomax model, the mean vorticity magnitude is used instead of the mean strain rate, although for two-dimensional boundary layers this substitution makes little difference. Major differences between the models exist in their treatments of the outer layer. As an example of a zero-equation model, consider the variation of the Cebeci-Smith model described in [28]. In the inner layer,

$$l_0 = \kappa y \left[1 - \exp(-\frac{y}{A})\right] \tag{4.18}$$

where κ is the von Karman constant (≈ 0.41), y is the vertical distance from the surface, and A is a damping coefficient such that

$$A = \frac{A^+ \mu}{\rho u_\tau \left(1 - 11.8 p^+\right)^{\frac{1}{2}}} \tag{4.19}$$

The friction velocity is u_τ, and

$$p^+ = -\frac{\mu_e U_e}{(\rho_e u_\tau^3)} \frac{dU_e}{dx} \tag{4.20}$$

is a nondimensional pressure-gradient parameter. The subscript e denotes a quantity evaluated at the boundary-layer edge. The mixing length l_0 is proportional to the distance from the wall. Close to the wall, the forces of molecular viscosity and the impermeability of the wall significantly reduce the turbulent shear stress and, through equations (4.15) and (4.17), the mixing length. The near-wall damping of the length scale is an important feature of many models; the complicated forms taken by some damping functions indicate efforts by modelers to account for various effects. Here, in addition to a van Driest damping, adjustments have been made to account for mean-flow pressure gradients. In the outer region of the boundary layer μ_t is given by

$$\mu_t = 0.0168 \ \rho\bar{\gamma} \left| \int_0^\infty (U_e - U) dy \right| \tag{4.21}$$

when the momentum-thickness Reynolds number Re_θ is greater than 5000. The quantity $\bar{\gamma}$ is an edge intermittency factor that smoothly reduces the eddy viscosity to zero outside the boundary layer. An Re_θ-dependent correction to the value of 0.0168 is applied when $Re_\theta < 5000$. The switch from inner to outer expression for eddy viscosity occurs at the smallest value of y at which the two expressions are equal. A typical distribution for the eddy viscosity, normalized by the molecular viscosity, is illustrated in figure 1. Note the discontinuous slope where the inner and outer models match.

4.2.2 One-Equation Models

In a one-equation model, a transport equation is solved for the turbulent kinetic energy. The velocity scale in the eddy viscosity is the square root of the turbulent kinetic energy, so

$$\mu_t = \bar{\rho}\nu_t = c_\mu \bar{\rho} k^{\frac{1}{2}} l_1 \tag{4.22}$$

where l_1 comes from an algebraic formula. For incompressible flow, the exact transport equation for k is

$$\frac{\partial k}{\partial t} + \bar{u}_i \frac{\partial k}{\partial x_i} = -\overline{u_i' u_j'} \frac{\partial \bar{u}_i}{\partial x_j} - \epsilon$$

$$-\frac{\partial}{\partial x_i}\left(\frac{1}{2}\overline{u_k' u_k' u_i'} + \frac{\overline{p' u_i'}}{\bar{\rho}}\right) + \nu\frac{\partial^2 k}{\partial x_j \partial x_j} \tag{4.23}$$

Unfortunately, some terms on the right side of equation (4.23) are not known and must be modeled. The turbulent transport is modeled by a gradient-diffusion hypothesis such that

$$\frac{1}{2}\overline{u_k' u_k' u_i'} + \frac{\overline{p' u_i'}}{\bar{\rho}} = -\left(\frac{\nu_t}{\sigma_k}\right)\frac{\partial k}{\partial x_i} \tag{4.24}$$

The dissipation term is also modeled, typically in a form

$$\epsilon = \frac{C^* k^{\frac{3}{2}}}{l_1} \tag{4.25}$$

Two distinct one-equation approaches are particularly relevant to transitional flows.

The Norris and Reynolds Approach

The Norris and Reynolds [29] model was developed in the early 1970's and then largely left unused until Rodi and his co-workers [30] at the University of Karlsruhe began using the model as part of a two-layer model. More details of the two-layer model will be discussed in the context of two-equation models.

The version of the Norris and Reynolds model that is used by the Karlsruhe group [30] is derived from the basic definitions for eddy viscosity (equ. (4.22)) and turbulent kinetic energy (equ. (4.23)) with the gradient-diffusion approximation for the pressure-velocity and triple-velocity correlations (equ. (4.24)). For consistency with the log layer, the constant c_μ in equation (4.22) is the square of twice the structure parameter $2a = -\overline{u'v'}/k$. For turbulent boundary layers in local equilibrium, experiments suggest that $2a = 0.3$; hence, $c_\mu = 0.09$. The constant σ_k in equation (4.24) is 1.0. The length scale l_1 varies linearly in the log-law region of the boundary layer (i.e., $l_1 = c_l y$). As in the Cebeci-Smith model, a near-wall (or perhaps more accurately, a low Reynolds number) damping is applied to the length scale. Different damping functions are used for μ_t and ϵ, so that

$$\mu_t = \bar{\rho}\nu_t = c_\mu \bar{\rho} k^{\frac{1}{2}} l_\mu \tag{4.26}$$

is the eddy viscosity and

$$\epsilon = \frac{k^{\frac{3}{2}}}{l_\epsilon} \tag{4.27}$$

is the dissipation, where

$$l_\mu = l_1 \left[1 - \exp\left(-\frac{R_y}{A_\mu} \frac{25}{A^+} \right) \right] \tag{4.28}$$

and

$$l_\epsilon = \frac{l_1}{\left(1 + \frac{5.3}{R_y} \right)} \tag{4.29}$$

are the damped length scales. The wall-normal Reynolds number

$$R_y \equiv \frac{k^{\frac{1}{2}} y}{\nu} \tag{4.30}$$

often appears in low Reynolds number damping functions. For conformity with the log-law layer, $c_l = \kappa c_\mu^{-3/4}$ where κ is the von Karman constant. The Karlsruhe group chooses $A_\mu = 50.5$ and $A^+ = 25$. Rodi [31] points out that the l_ϵ distribution is not in agreement with the DNS data very near the wall; however, this disagreement is unlikely to cause difficulties in computing quantities of engineering interest. Unlike many more complicated models, this model performs well under adverse pressure gradients [32].

The McDonald and Fish Route

In the early 1970's, McDonald and Fish [33] modified the one-equation model of McDonald and Camarata [34]. In both works the turbulent kinetic energy was integrated across the boundary layer; this integration eliminated the need to model the pressure-velocity and triple-velocity correlations and simplified the solution procedure. Algebraic models were developed for the remaining correlations. The structure parameter a was tuned for transitional flow. The model simulated the transition process in a variety of cases; the best comparisons to specific experiments occurred when the values used by the authors for free-stream turbulence and wall roughness differed from those values given by the experimenters. Shamroth and McDonald [35] made some adjustments to adapt the model for use in hypersonic boundary layers. Sometimes the agreement with experimental data was good and sometimes not. The modern

importance of this model is largely due to the recent resurrections of various aspects of the methodology.

Mavrantonakis and Grundmann [36] use many of the same closure assumptions as McDonald and Fish [33]; however, the differential (rather than integrated) form of the k equation is employed. The typical gradient-diffusion model (equation (4.24) with $\sigma_k = 1$) is used for the pressure-velocity and triple-velocity correlations. When the definition of the structure coefficient is used, the eddy viscosity is

$$\mu_t = \bar{\rho} l_\mu \sqrt{2 a_D k} \tag{4.31}$$

where the subscript D indicates streamwise damping. This use is consistent with equation (4.22) if $l_1 = l_\mu c_l / \kappa$ and c_l and c_μ are defined the same way as they were defined in the Norris and Reynolds approach.

The mixing-length variation across the boundary layer is adapted from McDonald and Camarata [34] as

$$\frac{l_\mu}{\delta} = \frac{(l_\mu)_e}{\delta} \tanh\left[\frac{\kappa y}{(l_\mu)_e}\right] \left[1.0 - \exp\left(-\frac{y^+}{A_D}\right)\right] \tag{4.32}$$

where the last expression in the brackets damps the length scale in the sublayer. Here $y^+ = y u_\tau / \nu$ where u_τ is the friction velocity and

$$A_D = \frac{26\,(l_\mu)_e}{0.085\delta} \tag{4.33}$$

The streamwise evolution of the length scale at the boundary-layer edge is taken from Deyhle and Grundmann [37] as

$$\frac{(l_\mu)_e}{\delta} = \frac{\int_0^\delta 2 a_D k \; dy}{\delta \int_0^\delta \frac{\partial U}{\partial y} \sqrt{2ak} \tanh\left[\kappa \frac{y}{(l_\mu)_e}\right]} \tag{4.34}$$

This expression must be solved iteratively.

Unlike other models that will be considered, ϵ in this case represents the true dissipation rate of k, which for incompressible flow can be written as

$$\epsilon = \nu \left(\overline{\frac{\partial u_i'}{\partial x_k} \frac{\partial u_i'}{\partial x_k}} + \overline{\frac{\partial u_i'}{\partial x_k} \frac{\partial u_k'}{\partial x_i}} \right) = \nu \overline{\frac{\partial u_i'}{\partial x_k} \frac{\partial u_i'}{\partial x_k}} + \nu \frac{\partial^2 \overline{u_i' u_k'}}{\partial x_k \partial x_i} \tag{4.35}$$

In other models, the second term is combined with viscous work terms to form $\nu\partial^2 k/\partial x_i \partial x_i$. For this particular model (and for other models in which ϵ is defined this way), the turbulent kinetic energy equation must be written

$$\frac{\partial k}{\partial t} + \bar{u}_i \frac{\partial k}{\partial x_i} = -\overline{u_i' u_j'} \frac{\partial \bar{u}_i}{\partial x_j} - \epsilon$$

$$- \frac{\partial}{\partial x_i}\left(\frac{1}{2}\overline{u_k' u_k' u_i'} + \overline{p' u_i'}\right) + \nu \frac{\partial}{\partial x_j}\left(\frac{\partial k}{\partial x_j} + \underline{\frac{\partial \overline{u_i' u_j'}}{\partial x_i}}\right) \tag{4.36}$$

The underlined term in equation (4.36) must also be modeled. Deyhle and Grundmann [37] account for this extra term, although the term is omitted in the more recent work of Mavrantonakis and Grundmann [36]. In either case, the two terms that make up ϵ are modeled separately as

$$\nu \overline{\frac{\partial u_i'}{\partial x_k}\frac{\partial u_i'}{\partial x_k}} = c_4 f_\epsilon \frac{(2a_D k)^{\frac{3}{2}}}{l_{\epsilon D}} \tag{4.37}$$

and

$$\nu \frac{\partial^2 \overline{u_i' u_k'}}{\partial x_k \partial x_i} = \left(\frac{l_\mu}{l_{\epsilon D}}\right)^2 (2a_D k) \frac{\partial \bar{u}_1}{\partial x_j} n_j \tag{4.38}$$

where

$$f_\epsilon = 1 - \exp\left(-0.01189 R_y\right) \tag{4.39}$$

is a low Reynolds number damping of the dissipation, n_j is the wall-normal unit vector, and $l_{\epsilon D}$ is the streamwise damped dissipation length scale. The nondimensional dissipation length scale is the same as that used by McDonald and Camarata [34], such that

$$\frac{l_\epsilon}{\delta} = 0.1 \tanh\left(\frac{\kappa y}{0.1}\right) \tag{4.40}$$

Intuitively, the term $\nu\left[\partial^2\left(\overline{u_i' u_k'}\right)/\partial x_k \partial x_i\right]$ in the dissipation should be modeled the same way as the underlined term in equation (4.36); however, Deyhle and Grundmann [37] model the two terms differently. Interestingly, Mavrantonakis and Grundmann [36] have traced some discrepancies in their skin-friction predictions to the dissipation rate, although they have not associated the problem with the inconsistency in their turbulent kinetic energy equation.

The transition process is largely accounted for by the streamwise damping functions. The damped structure constant is

$$a_D = \left[1.0 - \exp\left(-c_2\sqrt{\frac{(l_\mu)_e}{\delta}}\right)\right] a \tag{4.41}$$

and the damped dissipation length is

$$l_{\epsilon D} = \left[1.0 - \exp\left(-c_1\sqrt{\frac{(l_\mu)_e}{\delta}}\right)\right] l_\epsilon \tag{4.42}$$

where c_1 and c_2 depend on the free-stream turbulence level.

The model has been tested for flat plate and adverse-pressure-gradient boundary layers with $Tu \approx 1.2\%$ with a high degree of success; however, the results were not as encouraging for a three-dimensional boundary-layer case. A one-equation model is an efficient design tool, but this particular model needs further development with a more solid foundation for the dissipation rate.

4.2.3 Two-Equation Models

In two-equation models, transport equations are solved for both the velocity and length scales used to form the eddy viscosity. As in the one-equation model, the turbulent kinetic energy is used almost universally to obtain the velocity scale. A number of different approaches exist to determine the length scale. The most popular approach is to develop a transport equation for the dissipation ϵ, because ϵ appears explicitly in the k equation anyway. Various forms of the $k - \epsilon$ model will be discussed below. An alternative approach involves a transport equation for the turbulent time scale τ so that the turbulent length scale is proportional to $k^{1/2}\tau$. Speziale, Abid, and Anderson [38] have recently developed such a model; however, the model has been tested on only a small group of flows. Yet another choice is to develop a transport equation for ω, which is proportional to the dissipation rate per unit kinetic energy. Efforts to develop $k-\epsilon$ and $k-\omega$ models that are suitable for transition are underway; this section will focus on some details of these models for fully turbulent flow.

$k-\epsilon$ Models

In this approach

$$l_2 = f_\mu \frac{k^{\frac{3}{2}}}{\epsilon} \tag{4.43}$$

and the eddy viscosity can be written as

$$\mu_t = \bar{\rho}\nu_t = \bar{\rho}c_\mu k^{\frac{1}{2}} l_2 = \bar{\rho}c_\mu f_\mu \frac{k^2}{\epsilon} \tag{4.44}$$

the function f_μ has been included in anticipation of the need for a low Reynolds number damping function, as in the one-equation model. The exact equation for ϵ for incompressible flow is

$$\frac{\partial \epsilon}{\partial t} + \bar{u}_i \frac{\partial \epsilon}{\partial x_i} = \nu \nabla^2 \epsilon + \mathcal{P}_\epsilon + \mathcal{D}_\epsilon - \Phi_\epsilon \tag{4.45}$$

where the production of dissipation is

$$\begin{aligned} \mathcal{P}_\epsilon \equiv & -2\nu \overline{\frac{\partial u_i'}{\partial x_j}\frac{\partial u_k'}{\partial x_j}} \frac{\partial \bar{u}_i}{\partial x_k} - 2\nu \overline{\frac{\partial u_j'}{\partial x_i}\frac{\partial u_j'}{\partial x_k}} \frac{\partial \bar{u}_i}{\partial x_k} \\ & - 2\nu \overline{u_k' \frac{\partial u_i'}{\partial x_j}} \frac{\partial^2 \bar{u}_i}{\partial x_k \partial x_j} - 2\nu \overline{\frac{\partial u_i'}{\partial x_k}\frac{\partial u_i'}{\partial x_m}\frac{\partial u_k'}{\partial x_m}} \end{aligned} \tag{4.46}$$

the turbulent diffusion of dissipation is

$$\mathcal{D}_\epsilon \equiv -\nu \frac{\partial}{\partial x_k}\left(\overline{u_k' \frac{\partial u_i'}{\partial x_m}\frac{\partial u_i'}{\partial x_m}}\right) - 2\nu \frac{\partial}{\partial x_k}\left(\overline{\frac{\partial p'}{\partial x_m}\frac{\partial u_k'}{\partial x_m}}\right) \tag{4.47}$$

and the turbulent destruction of dissipation is

$$\Phi_\epsilon \equiv 2\nu^2 \overline{\frac{\partial^2 u_i'}{\partial x_k \partial x_m}\frac{\partial^2 u_i'}{\partial x_k \partial x_m}} \tag{4.48}$$

The last three terms of the ϵ equation need to be modeled. In the k equation, the turbulent diffusion of kinetic energy is approximated by a gradient-diffusion model. The same can be done for the turbulent diffusion of dissipation, such that $\mathcal{D}_\epsilon$ is approximated as

$$\mathcal{D}_\epsilon = \frac{\partial}{\partial x_i}\left(\frac{\nu_t}{\sigma_\epsilon}\frac{\partial \epsilon}{\partial x_i}\right) \tag{4.49}$$

where σ_ϵ is a constant.

The production of dissipation is modeled as

$$\mathcal{P}_\epsilon = -c_1 f_1 \left(\frac{\epsilon}{k}\right) \left(\overline{u_i' u_j'}\right) \frac{\partial \bar{u}_i}{\partial x_j} \tag{4.50}$$

where c_1 is a constant, and f_1 is a damping function. To obtain this form, the production of dissipation was assumed to be proportional to the production of turbulent kinetic energy. Recently, Speziale [39] showed that the same expression for $\mathcal{P}_\epsilon$ can be obtained by the less stringent assumption that the production of dissipation is governed by the level of anisotropy in the Reynolds stress tensor and the mean-velocity gradients. The leading order term in a Taylor-series expansion for small turbulent anisotropies and short turbulent time scales leads to equation (4.50).

Dimensional analysis suggests that the destruction of dissipation should be modeled as

$$\Phi_\epsilon = c_2 f_2 \frac{\epsilon^2}{k} \tag{4.51}$$

where c_2 is a constant, and f_2 is another damping function. Without any damping functions, this expression is singular at a solid surface because k (but not ϵ) goes to zero.

The value of the dissipation at a solid surface is

$$\epsilon|_{y=0} = \nu \left[\overline{(\frac{\partial u'}{\partial y})^2} + \overline{(\frac{\partial w'}{\partial y})^2}\right]_{y=0} = 2\nu \left(\frac{\partial \sqrt{k}}{\partial y}\right)^2_{y=0} \tag{4.52}$$

which is difficult to handle numerically because the boundary condition depends on the solution to the k equation. Several investigators get around this numerical difficulty by splitting the dissipation (i.e. $\epsilon = \tilde{\epsilon} + D$ where $\tilde{\epsilon}$ satisfies a homogeneous condition at the wall and D is a function that equals the wall value of the dissipation and goes to zero away from the wall). Additionally, an empirical source term E is sometimes added to the dissipation equation to increase the dissipation in certain areas of the flow.

When all of the pieces are put together, the standard incompressible $k-\epsilon$ model equations are

$$\frac{\partial k}{\partial t} + \bar{u}_i \frac{\partial k}{\partial x_i} =$$

$$- \overline{u_i' u_j'} \frac{\partial \bar{u}_i}{\partial x_j} - \epsilon + \frac{\partial}{\partial x_i} \left[\left(\nu + \frac{\nu_t}{\sigma_k} \right) \frac{\partial k}{\partial x_i} \right] \tag{4.53}$$

$$\frac{\partial \tilde{\epsilon}}{\partial t} + \bar{u}_i \frac{\partial \tilde{\epsilon}}{\partial x_i} =$$

$$+ c_1 f_1 \left(\frac{\tilde{\epsilon}}{k} \right) \left(-\overline{u_i' u_j'} \right) \frac{\partial \bar{u}_i}{\partial x_j} + \frac{\partial}{\partial x_i} \left[\left(\nu + \frac{\nu_t}{\sigma_\epsilon} \right) \frac{\partial \tilde{\epsilon}}{\partial x_i} \right] - c_2 f_2 \frac{\tilde{\epsilon}^2}{k} + E \tag{4.54}$$

with:

$$- \overline{u_i' u_j'} = \nu_t \left(\frac{\partial \bar{u}_i}{\partial x_j} + \frac{\partial \bar{u}_j}{\partial x_i} \right) - \frac{2}{3} k \delta_{ij} \tag{4.55}$$

and

$$\nu_t = c_\mu f_\mu \frac{k^2}{\tilde{\epsilon}} \tag{4.56}$$

In a comprehensive overview of the early $k-\epsilon$ models, Launder and Spalding [40] presented what have become fairly standard values for the various constants: $c_\mu = 0.09$, $c_1 = 1.44$, $c_2 = 1.92$, $\sigma_k = 1.0$, and $\sigma_\epsilon = 1.3$. The constant c_μ was determined by the requirement for a constant stress region; c_1, by the value of the von Karman constant; c_2, by comparison to experimental results of the decay of grid turbulence; and σ_k and σ_ϵ, by computer optimization. Launder and Spalding [40] avoid low Reynolds number, near-wall problems by not actually integrating the equations to the wall. Rather, Launder and Spalding assume a functional form of the solution in the near-wall region and match that with the solution at some point sufficiently far from the wall where the near-wall effects are negligible.

Jones and Launder [41] addressed the low Reynolds number and near-wall difficulties by using damping functions to multiply the standard values of c_μ (which multiplies the eddy viscosity) and c_2 (which multiplies the singular term in the ϵ equation). Jones and Launder chose

$$f_\mu = \exp \left[- \frac{2.5}{\left(1 + \frac{R_T}{50} \right)} \right] \tag{4.57}$$

and

$$f_2 = \left[1.0 - 0.3 \exp \left(-R_T^2 \right) \right] \tag{4.58}$$

where the turbulent Reynolds number is $R_T = k^2/(\tilde{\epsilon}\nu)$. They split the dissipation $\epsilon = \tilde{\epsilon} + D$ and used

$$D = 2\nu \left(\frac{\partial \sqrt{k}}{\partial y} \right)^2 \tag{4.59}$$

as well as a source term

$$E = 2\nu\nu_t \left(\frac{\partial^2 \overline{u_i}}{\partial x_j \partial x_j} \right) \left(\frac{\partial^2 \overline{u_i}}{\partial x_l \partial x_l} \right) \tag{4.60}$$

In the computed transition problem, transition occurred too abruptly at a Reynolds number that was too low. A minor variation of the Jones and Launder model was developed by Launder and Sharma [42], in which the damping function f_μ was changed to

$$f_\mu = \exp \left[-\frac{3.4}{\left(1 + \frac{R_T}{50}\right)^2} \right] \tag{4.61}$$

This change improved the performance of the model dramatically.

Lam and Bremhorst [43] developed a different set of wall functions to deal with low Reynolds number effects in the $k - \epsilon$ model. Their expression,

$$f_\mu = \left[1 - \exp\left(-0.0165 R_y\right)\right]^2 \left(1 + \frac{20.5}{R_T}\right) \tag{4.62}$$

was found by Patel, Rodi, and Scheuerer [44] to be a good approximation in the viscous region; however, the choice of $f_2 = 1 - \exp(-R_T^2)$ did not lead to the proper exponent for the final stages of decay of isotropic turbulence. The function $f_1 = 1 + (0.05/f_\mu)^3$ increased the dissipation and hence decreased the peak value of k in the near-wall region. The wall-boundary condition on the dissipation was taken from the k equation at the boundary (i.e., $\epsilon|_{y=0} = \nu \left(\partial^2 k/\partial y^2\right)|_{y=0}$). Patel, Rodi, and Scheuerer [44] found that

$$\left. \frac{\partial \epsilon}{\partial y} \right|_{y=0} = 0 \tag{4.63}$$

yielded almost identical results to those obtained with the use of the more complicated boundary conditions. Rodi and Scheuerer [17, 45] used this simplified boundary condition in their transitional flow calculations and obtained

reasonably good agreement with experimental measurements. However, like Jones and Launder [41], they found that the transition region was often too short.

In their two-layer model, Rodi and his coworkers [30, 31, 46, 47, 48] only use the $k-\epsilon$ model away from the wall region to avoid some of the near-wall problems associated with the $k-\epsilon$ model. Near the wall, the one-equation model of Norris and Reynolds [29] is used. This approach reduces the need for high resolution very near the wall, but is more empirical because the length-scale distribution must be prescribed algebraically. In addition, the two models must be matched at some distance from the wall. More details of this model will be described later when transitional flow modifications are discussed.

$k-\omega$ Models

As seen above, the ϵ equation has two important difficulties: the lack of natural boundary conditions for ϵ at the wall and the singularity of the ϵ^2/k term at the wall. Opportunities to resolve these problems are possible when the equation is recast in a different form.

Wilcox [49] reviews the history of $k-\omega$ models from 1942 until 1991. For the model that is discussed here, Wilcox [50] specifically assigns

$$\omega = \frac{\epsilon}{(\beta^* k)} \tag{4.64}$$

where β^* is a proportionality coefficient. The modeled forms of the k equation and ω equation are then written

$$\frac{\partial k}{\partial t} + \bar{u}_i \frac{\partial k}{\partial x_i} =$$

$$-\overline{u_i' u_j'} \frac{\partial \bar{u}_i}{\partial x_j} - \beta^* k\omega + \frac{\partial}{\partial x_i}\left[\left(\frac{\nu_t}{\sigma_k}\right)\frac{\partial k}{\partial x_i}\right] + \nu \frac{\partial^2 k}{\partial x_j \partial x_j} \tag{4.65}$$

and

$$\frac{\partial \omega}{\partial t} + \bar{u}_i \frac{\partial \omega}{\partial x_i} = \nu \frac{\partial^2 \omega}{\partial x_j \partial x_j}$$

$$+ \alpha \frac{\omega}{k}\left(-\overline{u_i' u_j'}\right)\frac{\partial \bar{u}_i}{\partial x_j} + \frac{\partial}{\partial x_i}\left[\left(\frac{\nu_t}{\sigma_\omega}\right)\frac{\partial \omega}{\partial x_i}\right] - \beta\omega^2 \tag{4.66}$$

with

$$\nu_t = \frac{\alpha^* k}{\omega} \tag{4.67}$$

The coefficients σ_k and σ_ω are both set equal to 2. In the high Reynolds number version of the model, $\alpha = 5/9$, $\alpha^* = 1$, $\beta^* = 9/100$, and $\beta = 3/40$. According to Wilcox [49], even though the asymptotic behavior as $y \to 0$ is not correct ($\overline{u'v'} \sim y^4$ rather than $\overline{u'v'} \sim y^3$), this model predicts the mean-flow profiles for adverse-pressure-gradient flows better than $k - \epsilon$ models. Wilcox [49] believes that the proper behavior in the defect layer is more important than in the sublayer. Additional modifications for transitional flow will be discussed later.

Summary of Two-Equation Turbulence Models

A limited sample of the rich variety of two-equation turbulence models is offered above. Much of the diversity in these models is generated by the low Reynolds number forms of $k - \epsilon$ models. To sort through the numerous possibilities, Patel, Rodi, and Scheuerer [44] evaluated eight different two-equation low Reynolds number turbulence models. The desired mathematical properties of the models, as well as their actual performance on four carefully chosen test cases, were discussed.

The low Reynolds number functions f_μ, f_1, f_2, D, and E are incorporated into the modeled equations for different reasons. The reduction in the shear stress by the function f_μ as the wall is approached is the result of two independent phenomena: the direct action of molecular viscosity and the near-wall influence on the fluctuating pressure. The second phenomenon is actually independent of viscosity and should not be correlated with R_T, R_y, or y^+. However, because the separation of the two effects in the resulting shear stress is difficult, the effects are usually modeled together. Experimental evidence suggests that f_μ should asymptote to unity by $y^+ = 60$, although all models tested asymptoted beyond this point. The functions f_1 and f_2 control, respectively, the near-wall changes in the production and destruction of ϵ. The presence of f_1 increases ϵ in the vicinity of the wall. The additional function E is used for a similar purpose. The presence of f_2 is occasionally required to stabilize the numerical solution of the ϵ equation as $k \to 0$, in which case $f_2 \propto y^2$ near the wall. The use of an alternative dissipation function $\tilde{\epsilon} = \epsilon - D$, where $D \neq 0$ (as in the Jones and Launder

model), sometimes eliminates this difficulty (typically at the cost of introducing an accuracy problem right near the wall, because $\tilde{\epsilon}$ usually varies much more rapidly than ϵ in the wall region). The function f_2 is based on an experimentally observed change in the decay law of isotropic turbulence from $k \propto x^{-1.25}$ to $k \propto x^{-2.5}$ as the turbulence intensity R_T decreases. The effect of f_2 should be restricted to low R_T (typically $R_T < 15$).

The computations performed by Patel, Rodi, and Scheuerer [44] revealed that some models did not produce results consistent with experiments even for the zero-pressure-gradient test case. An analysis of the near-wall behavior of several turbulence quantities suggested that the constants and damping functions used in those models (Hassid-Poreh [51], Hoffman [52], Dutoya-Michard [53], and Reynolds [54]) restricted their generality. The models of Launder and Sharma [42], Chien [55], Lam and Bremhorst [43], and Wilcox and Rubesin [56] performed much better, although even these needed improvement. Patel, Rodi, and Scheuerer suggested that

1. The damping function f_μ be chosen to agree with available experimental data and its effects restricted to the sublayer and buffer zones.

2. The functions f_1 and f_2 in the dissipation-rate equation should be mathematically consistent with the required near-wall behavior.

3. All functions and constants should be fine-tuned to reproduce the basic features of wall-bounded shear flows in a variety of pressure gradients.

Finally, Patel, Rodi, and Scheuerer [44] note that modifications to the high Reynolds number versions of most models will be required to handle adverse-pressure-gradient flows.

4.3 Reynolds Stress Transport Turbulence Models

Most two-equation models have trouble with stagnation flows because the turbulent energy production is dominated by the normal, rather than the shear stresses, and the normal stresses are typically not calculated properly with an isotropic eddy-viscosity model. In addition, two-equation models do not consider the effects of curvature and rotation (and body forces in

general) on the turbulence structure, which creates the need for a higher level of modeling.

The Reynolds stress transport (RST) models are also known as Reynolds stress closures, second-order closures, and second-moment closures. The term Reynolds stress transport will be used here. These models do not assume an eddy viscosity, but rather use transport equations for all of the terms of the Reynolds stress tensor. For incompressible flows

$$\frac{\partial\left(\overline{u_i'u_j'}\right)}{\partial t} + \bar{u}_k\frac{\partial\left(\overline{u_i'u_j'}\right)}{\partial x_k}$$

$$= P_{ij} + \Pi_{ij} - \epsilon_{ij} - \frac{\partial C_{ijk}}{\partial x_k} + \nu\frac{\partial\left(\overline{u_i'u_j'}\right)}{\partial x_k\partial x_k} \tag{4.68}$$

where the production of turbulent stress is

$$P_{ij} = -\left(\overline{u_i'u_k'}\right)\frac{\partial\bar{u}_j}{\partial x_k} - \left(\overline{u_j'u_k'}\right)\frac{\partial\bar{u}_i}{\partial x_k} \tag{4.69}$$

the pressure-strain correlation is

$$\Pi_{ij} \equiv \overline{\frac{p'}{\rho}\left(\frac{\partial u_i'}{\partial x_j} + \frac{\partial u_j'}{\partial x_i}\right)} \tag{4.70}$$

the dissipation-rate correlation is

$$\epsilon_{ij} \equiv 2\nu\overline{\frac{\partial u_i'}{\partial x_k}\frac{\partial u_j'}{\partial x_k}} \tag{4.71}$$

and the turbulent-stress-diffusion correlation is

$$C_{ijk} \equiv \overline{u_i'u_j'u_k'} + \overline{p'u_i'}\delta_{jk} + \overline{p'u_j'}\delta_{ik} \tag{4.72}$$

As an example of an RST closure, the model presented by Savill [57] will be considered. The model contains many features of the model developed by Kebede, Launder, and Younis [58]. As is often done, a gradient-diffusion hypothesis is used to model the turbulent diffusion of turbulent stress

$$C_{ijk} = -c_s\frac{k}{\epsilon}\overline{u_k'u_l'}\frac{\partial\overline{u_i'u_j'}}{\partial x_l} \tag{4.73}$$

Note that this choice is not symmetric with respect to an interchange of either i or j with k. Launder and Shima [59] use the same approximation for this term and point out that the choice is made for computational convenience rather than accuracy. Because of the relative unimportance of diffusive transport, Launder and Shima [59] maintain that the errors are unlikely to have a significant effect. The modeled dissipation-rate correlation is

$$\epsilon_{ij} = \epsilon \left[\frac{2}{3}\delta_{ij}\left(1 - f_s\right) + \frac{F f_s}{k}\left(\overline{u_i' u_j'} + \overline{u_i' u_k'} n_k n_j + \overline{u_j' u_k'} n_k n_i - \delta_{ij}\overline{u_k' u_l'} n_k n_l\right)\right] \tag{4.74}$$

where

$$f_s = \frac{1}{1 + \frac{R_T}{10}} \tag{4.75}$$

is a function that goes to one with low turbulence Reynolds numbers and goes to zero with high turbulence Reynolds numbers. The function

$$F = \frac{1}{1 + 2.5\frac{\overline{u_2'^2}}{k}} \tag{4.76}$$

ensures that the tensor contracts properly. The long expression, multipled by $f_s F$, yields the proper limiting behavior as the wall is approached. The pressure-strain correlation is modeled with four terms:

$$\Pi_{ij} = \Pi_{ij1} + \Pi_{ij1}^w + \Pi_{ij2} + \Pi_{ij2}^w \tag{4.77}$$

Here,

$$\Pi_{ij1} = -c_1 \epsilon a_{ij} \tag{4.78}$$

where $a_{ij} = (\overline{u_i' u_j'} - 2/3\delta_{ij}k)/k$ is the anisotropic part of the Reynolds stress and

$$\Pi_{ij2} = -c_2\left(P_{ij} - \frac{1}{3}\delta_{ij}P_{kk}\right) \tag{4.79}$$

models the fully turbulent portion of the pressure strain. The wall functions Π_{ij1}^w and Π_{ij2}^w are only important near solid boundaries, where they redistribute velocity fluctuations from those normal to the wall to those parallel to the wall. These functions are modeled as

$$\Pi_{ij1}^w = c_1^w(\frac{\epsilon}{k})\left(\overline{u_k' u_m'} n_k n_m \delta_{ij} - \frac{3}{2}\overline{u_k' u_i'} n_k n_j - \frac{3}{2}\overline{u_k' u_j'} n_k n_i\right) f \tag{4.80}$$

and

$$\Pi_{ij2}^{w} = c_2^{w}\left(\Pi_{km2}n_k n_m \delta_{ij} - \frac{3}{2}\Pi_{ik2}n_k n_j - \frac{3}{2}\Pi_{jk2}n_k n_i\right) f \tag{4.81}$$

where the near-wall damping function is $f = k^{3/2}/(\epsilon x_2)$ with x_2 equal to the distance to the wall. The recommended constants are $c_1 = 1.8$, $c_2 = 0.6$, $c_1^w = 0.5$, and $c_2^w = 0.3$. The dissipation-rate equation used is

$$\frac{D\epsilon}{Dt} = \frac{\partial}{\partial x_k}\left[\left(c_\epsilon \frac{k}{\epsilon}\overline{u_k' u_l'} + \nu\delta_{kl}\right)\frac{\partial \epsilon}{\partial x_l}\right] + f_1 c_{\epsilon 1}\left(\frac{\epsilon}{k}\right)\frac{P_{kk}}{2} - f_2 c_{\epsilon 2}\frac{\epsilon\tilde{\epsilon}}{k} + E \tag{4.82}$$

with

$$\tilde{\epsilon} = \epsilon - 2\nu\left(\frac{\partial k^{\frac{1}{2}}}{\partial x_l}\right)\left(\frac{\partial k^{\frac{1}{2}}}{\partial x_l}\right) \tag{4.83}$$

and wall damping functions

$$f_1 = \max\left[\frac{1}{c_{\epsilon 1}}\left(2.0 - \frac{0.725 R_y}{65}\right), 1\right] \tag{4.84}$$

$$f_2 = \min\left[1 - \frac{0.4}{c_{\epsilon 2}}\exp\left(\frac{R_T}{6}\right)^2, 20\right] \tag{4.85}$$

An additional source term for dissipation is included. This source term accounts for the third term on the right side of equation (4.46) and takes the form

$$E = f_\mu c_{\epsilon 3}\nu\frac{\overline{u_j' u_k'}}{k}\frac{k^2}{\epsilon}\frac{\partial^2 \bar{u}_i}{\partial x_j \partial x_l}\frac{\partial^2 \bar{u}_i}{\partial x_k \partial x_l} \tag{4.86}$$

where the damping function f_μ is the same as that used in the Launder and Sharma [42] near-wall $k-\epsilon$ model:

$$f_\mu = \exp\left[-\frac{3.4}{\left(1 + \frac{R_T}{50}\right)^2}\right] \tag{4.87}$$

The constants used are $c_\epsilon = 0.15$, $c_{\epsilon 1} = 1.275$, $c_{\epsilon 2} = 1.8$, and $c_{\epsilon 3} = 0.25$. Some constants and functions have been developed with thought to the physics, or at least the statistics, of turbulent flows; however, many are ad hoc and have been optimized by comparisons of mean-flow features of computer calculations with specific experimental results. Therefore, the generality of the model is somewhat questionable. However, this model performs well for transitional flows and is discussed in Chapter 6.

4.4 Large-Eddy Simulation

In large-eddy simulation, the large-scale quantities are defined by a filtering operation

$$f = \bar{f} + f' \tag{4.88}$$

where

$$\overline{f}(\mathbf{x}, t) = \int f(\mathbf{x}^*, t) G(\mathbf{x}, \mathbf{x}^*) d\mathbf{x}^* \tag{4.89}$$

The integral is extended over the entire spatial domain, and G is a filter function. Unlike the RANS equations, the overbar here represents the time-dependent large scales of motion rather than a time average or an ensemble mean. Primed quantities denote a SGS component of the flow. For the incompressible isenthalpic case, the filter applied to the Navier-Stokes equations (equ. (4.1)) and the continuity equation (equ. (4.2)) yields the filtered equations

$$\frac{\partial \bar{u}_i}{\partial t} + \frac{\partial \left(\bar{u}_i \bar{u}_j \right)}{\partial x_j} = -\frac{\partial \bar{p}}{\partial x_i} - \frac{\partial \tau_{ij}}{\partial x_j} + \frac{1}{Re} \frac{\partial^2 \bar{u}_i}{\partial x_j \partial x_i} \tag{4.90}$$

and

$$\frac{\partial \bar{u}_i}{\partial x_i} = 0 \tag{4.91}$$

where a reference length and velocity have been used to nondimensionalize all quantities and produce the Reynolds number. The SGS stress

$$\tau_{ij} \equiv \overline{u_i u_j} - \overline{u_i}\ \overline{u_j} \tag{4.92}$$

is not known and must be modeled. Note that although the large-eddy equations of motion look much like the Reynolds-averaged equations, the meaning is different. In the Reynolds-averaged equations, the computed mean quantities are a time average or an ensemble average. In either case, all of the turbulent motion is buried in the Reynolds stress. However, in LES, the averages are spatial averages where the modeled parts are those motions that occur on scales that are too small to be resolved on the grid. In a properly performed LES, all important temporal variations in the flow are explicitly calculated, this includes the evolution of the turbulent motion (i.e., the large eddies). Traditional thinking assumes that the SGS features simply transfer energy to higher wave numbers where the energy can be dissipated.

A common approach is to employ an eddy-viscosity model for the small scales so that the modeled SGS stress can be written as

$$\tau_{ij} = -2\nu_t \overline{S_{ij}} + \frac{2}{3}\delta_{ij} k_{\text{sgs}} \tag{4.93}$$

where k_{sgs} is the SGS kinetic energy and $\overline{S}_{ij}$ is the large-scale strain-rate tensor. A Smagorinsky [60] model is typically used for the eddy viscosity to yield

$$\nu_t = C_s \Delta^2 \bar{S} \tag{4.94}$$

where $\bar{S} = \sqrt{2\bar{S}_{ij}\bar{S}_{ij}}$, Δ is a length scale which is the geometric mean of the grid spacings in the three coordinate directions, and C_s is the square of the usual Smagorinsky coefficient. Although C_s has traditionally been taken as a constant, no necessity exists for it to be constant, nor must it be positive everywhere as was the original Smagorinsky constant. In fact, recent DNS work done by Piomelli, Cabot, Moin, and Lee [61] suggests that energy transfer from the subgrid scales to the large scales occurs at nearly as many grid points as does energy transfer from the large scales to the subgrid scales. Of course, for any statistically steady turbulent flow, the net energy transfer must be from the large scales to the subgrid scales; however, the energy transfer can also be in the opposite direction. This phenomenon is known as backscatter. Germano, Piomelli, Moin and Cabot [62] used this insight to develop the "dynamic subgrid scale model" for LES. In this model, two filtering operators are used:

$$\overline{f}(\mathbf{x}) = \int f(\mathbf{x}')\overline{G}(\mathbf{x},\mathbf{x}')d\mathbf{x}' \tag{4.95}$$

where $\overline{G}$ is the grid filter, and

$$\tilde{f}(\mathbf{x}) = \int f(\mathbf{x}')\tilde{G}(\mathbf{x},\mathbf{x}')d\mathbf{x}' \tag{4.96}$$

where $\tilde{G}$ is the test filter. All integrations are performed over the entire computational domain. The test filter corresponds to a coarser mesh than the grid filter. The combination filter $\tilde{\bar{G}} = \tilde{G}\bar{G}$ also can be applied to the original equations of motion. This application results in an equation similar to the one that describes the large eddies; however, the overbar terms now have an additional tilde on top and the SGS stress is now written as

$$T_{ij} = \widetilde{\overline{u_i u_j}} - \tilde{\bar{u}}_i \tilde{\bar{u}}_j \tag{4.97}$$

The smallest of the resolved stresses are represented by

$$\mathcal{L}_{ij} = \widetilde{\bar{u}_i \bar{u}_j} - \tilde{\bar{u}}_i \tilde{\bar{u}}_j \tag{4.98}$$

which can also be written as

$$\mathcal{L}_{ij} = T_{ij} - \tilde{\tau}_{ij} \tag{4.99}$$

When a Smagorinsky model is used for both T_{ij} and τ_{ij}, the anisotropic parts of T_{ij} and τ_{ij} are

$$T_{ij} - (\frac{\delta_{ij}}{3})T_{kk} \approx M_{ij} = -2C_s \tilde{\bar{\Delta}}^2 \tilde{\bar{S}} \tilde{\bar{S}}_{ij} \tag{4.100}$$

and

$$\tau_{ij} - (\frac{\delta_{ij}}{3})\tau_{kk} \approx m_{ij} = -2C_s \overline{\Delta}^2 \bar{S} \bar{S}_{ij} \tag{4.101}$$

where $\tilde{\bar{\Delta}}$ and $\overline{\Delta}$ are the filter widths associated with $\tilde{\bar{G}}$ and $\bar{G}$, respectively. When equation (4.99) is contracted with $\bar{S}_{ij}$ and the modeled expressions are used,

$$\mathcal{L}_{ij} \bar{S}_{ij} = -2C_s \left(\tilde{\bar{\Delta}}^2 \tilde{\bar{S}} \tilde{\bar{S}}_{ij} \bar{S}_{ij} - \overline{\Delta}^2 \widetilde{\bar{S}\bar{S}_{ij}} \bar{S}_{ij} \right) \tag{4.102}$$

is obtained, which can be solved for the Smagorinsky coefficient C_s. However, because the quantity in parentheses can become zero, in practice C_s is assumed to be a function only of the wall-normal distance and time. Planar averages are used for the terms in the parentheses. This model has been used with some success in both fully turbulent and transitional flows.

The model has been extended to compressible flow by Moin, Squires, Cabot, and Lee [63]. The density must be included in the stress tensors, and an SGS heat-flux vector

$$\dot{q}_k = \overline{\rho u_k T} - (\frac{1}{\bar{\rho}}) \overline{\rho u_k} \, \overline{\rho T} \tag{4.103}$$

is modeled in much the same way as the SGS stress.

Another formulation of the model has been proposed by Lilly [64] in which the tensor $\mathcal{L}_{ij}$ is contracted with M_{ij} instead of $\bar{S}_{ij}$. A positive-definite expression is ensured for the poorly behaved term in equation (4.102); however, tests show that despite its positive definiteness, the term remains ill-behaved. As a result, spatial averages are still employed.

Chapter 5

Transition-Region Models

5.1 Linear-Combination Transition-Region Models

In a linear-combination transition-region model, estimates of turbulent flow-field quantities are linearly combined with estimates of the corresponding laminar flow-field quantities. The proportion of each of these estimates is determined by the intermittency of the flow. For example,

$$\bar{u}_i = (1-\gamma)\,(\bar{u}_i)_{\text{lam}} + \gamma\,(\bar{u}_i)_t \tag{5.1}$$

where the subscripts lam and t indicate the estimate for the laminar and turbulent flows, respectively.

This kind of transition model can be traced to Emmons [65] and his classic work on turbulent spots. Dhawan and Narasimha [66] later discovered that the intermittency distribution in constant-pressure transitional boundary layers could be correlated by the expression

$$\gamma = 1 - \exp\left[-0.411\left(\frac{x - x_{t0}}{\lambda}\right)^2\right] \tag{5.2}$$

where λ is the streamwise distance between the points at which $\gamma = 0.25$ and $\gamma = 0.75$, and x_{t0} is the location where the intermittency first becomes nonzero. However, the values of x_{t0} and λ varied within individual experiments so that the correlation alone could not be used to predict transition.

Chen and Thyson [67] proposed a different intermittency distribution to account for pressure gradient and compressibility effects, although Narasimha [68] later claimed that this formulation was not well supported by experimental data. Instead, Narasimha [69] and Dey and Narasimha [70] proposed that subtransitions, or breaks in the usual Dhawan and Narasimha [66] correlation exist in flows with strong pressure gradients. Dey and Narasimha [18] used the subtransition concept to correlate flows with pressure gradients by combining two sets of transition start and end locations.

To develop a useful model, both x_{t0} and λ must be known. In the linear-combination model proposed by Dey and Narasimha [18] the starting location of transition must be determined by some other means (e.g., an e^N method) and empirical correlations must be used to determine λ. (See also reference [71] for a concise summary and additional references.)

The point x_{t0} is the origin of the turbulent boundary layer. The unknown distance λ is obtained from

$$\lambda = \left[0.411 \frac{Re_\theta^3(x_{t2})}{N_2}\right]^{\frac{1}{2}} \frac{\nu}{U_e(x_{t2})} \tag{5.3}$$

where ν is the kinematic viscosity at the edge of the boundary layer, $U_e(x_{t2})$ is the boundary-layer-edge velocity at x_{t2}, and Re_θ is the Reynolds number based on laminar momentum thickness at the point x_{t2}. For mild pressure gradients, $x_{t2} = x_{t0}$. For stronger pressure gradients, x_{t2} must be determined from the intermittency distribution. Because no correlation exists for finding x_{t2}, $x_{t2} = x_{t0}$ is used to predict the intermittency distribution with this model. The factor N_2 is a nondimensional turbulent-spot formation rate and is determined from the correlation

$$N_2 = N_0(M, q) + 0.24 L_{t2}^2 \qquad (L_{t2} > 0) \tag{5.4}$$

or

$$N_2 = N_0(M, q) - 323.0 L_{t2}^3 \qquad (L_{t2} < 0) \tag{5.5}$$

where $N_0 = 0.7 \times 10^{-3}$ for incompressible flows with a free-stream turbulence level Tu greater than 0.2%, and L_{t2} is a pressure-gradient parameter that is equal to $dU_e/dx\ \theta_{\text{lam}}^2/\nu$. Both the free-stream velocity gradient dU_e/dx and the laminar momentum thickness θ_{lam} are measured at x_{t2}. For compressible flows, the Mach number correction to N_0 given by Narasimha [68] is used.

Very low free-stream turbulence levels require a modified value of N_0. The modification

$$N_0 = -1.453 \times 10^{-3} \log(Tu) - 1.61 \times 10^{-3} \qquad (Tu < 0.2\%) \tag{5.6}$$

results when a curve is fitted to the data in Figure 5.10 of Dey and Narasimha [18].

5.2 Algebraic Transition-Region Models

In algebraic models, the mean flow is calculated from a set of averaged equations in which the effective viscosity μ_{eff} is equal to the sum of the molecular viscosity μ and the product of a transition function γ_t and a turbulent eddy viscosity μ_t, such that

$$\mu_{\text{eff}} = \mu + \gamma_t \, \mu_t \tag{5.7}$$

The turbulent eddy viscosity μ_t may be determined from any type of turbulent eddy-viscosity model. The transition function γ_t is **not** the intermittency of the flow, but an empirically determined expression that indicates the appropriate fraction of the fully turbulent eddy viscosity. For purposes here, assume that the appropriate starting location for transition has been determined by some other means. The model must determine the value of γ_t. One model, developed at ONERA/CERT, uses a correlating parameter that depends on the momentum thickness of the flow and the Mach number at the edge of the boundary layer [72, 73, 24]. Specifically,

$$\chi_1 = \frac{\frac{\theta}{\theta_{t0}} - 1 + 0.005 M_e^2}{1 + 0.02 M_e^2} \tag{5.8}$$

where θ_{t0} is the momentum thickness at the point where the model is started. The expression for γ_t is piecewise continuous in the streamwise direction and is constant across the boundary layer. The algebraic expressions for γ_t that have been used in recent tests of this model [74, 28, 75] are given by Arnal (private communication).
For $0 < \chi_1 \leq 0.25$,

$$\gamma_t = 1 - \exp\left\{-4.5 \left[\chi_1 \left(1 + 0.02 M_e^2\right) - 0.005 M_e^2\right]^2\right\} \tag{5.9}$$

For $0.25 < \chi_1 \leq 0.75$,

$$\gamma_t = 18.628\chi_1^4 - 55.388\chi_1^3 + 52.369\chi_1^2 - 16.501\chi_1 + 1.893 \tag{5.10}$$

For $0.75 < \chi_1 \leq 3$,

$$\gamma_t = 1.25 - 0.25 \sin\left[\pi\left(0.444\chi_1 - 0.833\right)\right] \tag{5.11}$$

For $\chi_1 > 3$,

$$\gamma_t = 1 \tag{5.12}$$

Note that the transition function exceeds unity for part of the region so cannot represent the true intermittency of the flow.

Data of low-speed flows with zero and mildly adverse pressure gradients were used to develop the ONERA/CERT model. This model works quite well in predicting the length of the transition region for these flows [28, 74]. As with all linear-combination and algebraic transition-region models, no absolute criterion exists for determining the location at which the model is initiated. For comparison with experimental data, Singer, Dinavahi, and Iyer [28] and Singer, Dinavahi and Zang [74] initiated the transition-region model at an x-Reynolds number approximately equal to 91% of the x-Reynolds number that corresponds to a local minimum in a surface quantity (e.g., skin friction or heat flux). The choice of this x-Reynolds number was based on *posteriori* optimization in the case of Singer, Dinavahi, and Zang [74] and based on a suggestion by Dey and Narasimha [18] for the Singer, Dinavahi, and Iyer report [28]. Although this guideline for the initiation position generally leads to reasonable answers, it is not foolproof. In figure 2 the ONERA/CERT model is used with three different starting locations, and the results are compared to the experimental findings of Kimmel (personal communication) for the flow over a cold-wall cone at a Mach number of 8. The 91% guideline corresponds to $R_{t0} = 2.3 \times 10^6$. The model's performance here is not encouraging; however, if the third and fifth experimental data points were in error (a reasonable assumption), then the curve with $R_{t0} = 3.0 \times 10^6$ would be appropriate. Note that in this curve, the maximum Stanton number has been reduced, and the model and experimental results agree better. Finally, when the model is started further downstream with $R_{t0} = 3.6 \times 10^6$, the resulting curve is the closest to the experimental data in the transition zone. In a practical application of the model, the experimental data would

not be available to optimize the starting location. Singer, Dinavahi, and Zang [74] show that an e^N approach with $9 < N < 10$ provides appropriate starting locations for supersonic flight-test data, although the margin of error is large (perhaps from 15 to 20% discrepancies in the optimal choice of R_{t0}).

A serious problem with the ONERA/CERT model occurs with strong favorable pressure gradients, where the momentum thickness decreases with streamwise distance. In these cases, the model can fail to transition properly. For example, consider figure 3, which is plotted with data from reference [28] and digitized data from reference [46]. This flow involved a strong favorable pressure gradient with a free-stream turbulence level of about 2%. (See Blair and Werle [76] for experimental details.) The chain-dashed line illustrates the Stanton number distribution for this flow when the two-layer model of Fujisawa, Rodi, and Schönung [46] is used. This model will be discussed later. The dashed line (concealed by the solid line in the laminar region) represents the results from the linear-combination model of Dey and Narasimha. (See previous section.) The solid line is the Stanton number computed with the ONERA/CERT algebraic model. The laminar momentum thickness in this flow began to decrease slightly upstream of the Stanton number minimum. Although the transition model was initiated, the decreasing laminar momentum thickness prevented any turbulent eddy viscosity from being added; hence, the calculated flow remained laminar throughout the test section.

5.3 Differential Transition-Region Models

Turbulence models have been used to model the transition region for several decades. Donaldson [77] solved a form of RST equations (he solved for three normal stresses and τ_{xy}) for transitional flows. He computed the onset and evolution of transitional flow and performed many computations that demonstrated the effects of various model constants, starting locations, and initial profiles; however, he did not present comparisons with specific experiments.

Launder and Spalding [40] reported the results of some $k-\epsilon$ calculations by Priddin [78] in which the transitional flow over a turbine blade at various levels of free-stream turbulence was accurately calculated. Launder and Spalding [40] suggested that "the low Reynolds number form of the $k-\epsilon$ model has its own built-in 'transition criterion.' "

A somewhat different view has evolved since then. The transport equa-

tions associated with turbulence models allow for the transport of free-stream turbulence into a laminar boundary layer. When the level of free-stream turbulence is sufficiently high, the rate of diffusion of this free-stream turbulence into the boundary layer can exceed its dissipation rate. At some point, the turbulence model production mechanisms respond to the free-stream turbulence that has diffused into the boundary layer in the same way these mechanisms would respond to genuine turbulence; a pseudotransition process occurs, and the end result is a turbulent boundary layer.

The pseudotransition process is sensitive to a number of details in the calculations, particularly the starting profiles of various quantities (k and ϵ, where appropriate, or the Reynolds stresses for RST models) and the streamwise position where the models are started. Detailed studies of the physical processes of transition amid high levels of free-stream turbulence have not yet established the relationship of the pseudotransition in the models to the true physical processes. The suggestion that the models simulate the physical transition process (even in the case of high free-stream turbulence) is premature, if not completely incorrect. The fact that reasonable results are obtained in some cases from models that are not explicitly designed for transitional flow is largely fortuitous.

Schmidt and Patankar [79] performed extensive tests with the $k-\epsilon$ models of Jones and Launder [41] and Lam and Bremhorst [43] to determine the suitability of the models for simulating boundary-layer transition. Schmidt and Patankar [79] contend that low Reynolds number $k-\epsilon$ models can reproduce some qualitative aspects of boundary-layer transition because of the weak correspondence between a developing laminar boundary layer and the viscous sublayer, the transitional flow region and the buffer layer, and the fully turbulent boundary layer and the "law of the wall" region. After the models were tested, the authors concluded that

1. The predicted starting location of transition is moderately sensitive to initial profiles for k and ϵ and the location at which the calculations begin. This sensitivity will be discussed in more detail later.

2. Basic qualitative aspects of transition are correct (i.e., the higher the turbulence level, the earlier transition begins); however, when the calculations start early so that sensitivity to the starting location and profiles decreases, transition is consistently predicted unrealistically early.

3. The transition lengths are significantly shorter than those found in experiments.

These conclusions are consistent with the findings of other modelers [80, 45]. In addition to the problems identified thus far, Rodi [30] indicates that the models only undergo transition with high ($> 1\%$) free-stream turbulence levels. The low free-stream turbulence case must be dealt with in a different way.

This section covers models in which the transport equations have been altered to specifically account for the transition process. Most of these modifications are empirical; hence, they can be applied only to the regime for which the empirical correlations have been formulated.

One set of experiments performed by Abu-Ghannam and Shaw [81] in incompressible flow with pressure gradients and free-stream turbulence is commonly used to calibrate the models. Abu-Ghannam and Shaw [81] correlated the beginning and ending transition Reynolds numbers for many flows and presented these correlations:

$$Re_{\theta s} = 163 + \exp\left[F\left(\lambda_\theta\right)\left(1 - \frac{Tu}{6.91}\right)\right] \tag{5.13}$$

for the start of transition and

$$Re_{\theta e} = 540 + 183.5\left(R_L \times 10^{-5} - 1.5\right)\left(1 - 1.4 - \lambda_\theta\right) \tag{5.14}$$

for the end of transition. In these expressions, $\lambda_\theta = (\theta^2/\nu)dU_e/dx$, and R_L is a length Reynolds number given by

$$R_L = 16.8(Re_{xs})^{0.8} \tag{5.15}$$

where Re_{xs} is the x-Reynolds number of the start of transition. The function $F(\lambda_\theta)$ is given by

$$F(\lambda_\theta) = 6.91 + 12.75\lambda_\theta + 63.64\lambda_\theta^2 \qquad (\lambda_\theta \leq 0) \tag{5.16}$$

and

$$F(\lambda_\theta) = 6.91 + 2.48\lambda_\theta - 12.27\lambda_\theta^2 \qquad (\lambda_\theta > 0) \tag{5.17}$$

The beginning and ending Reynolds numbers from the Abu-Ghannam and Shaw [81] experiments were determined by measurements with a single, fixed probe and varying free-stream conditions.

5.3.1 The Two-Layer $k-\epsilon$ Model

Chapter 4 briefly described the two-layer approach of Rodi [31] in which a standard $k-\epsilon$ model was used for the bulk of the flow, and a version of the Norris and Reynolds [29] one-equation model was used for the near-wall region. The parameter A^+, which is used in the damping of the turbulence transport length scale, is used to control the transition process. Thus,

$$A^+ = A_t^+ + \left(300 - A_t^+\right)\left[1 - \sin\left(\frac{\pi}{2}\frac{Re_\theta - Re_{\theta s}}{Re_{\theta s}}\right)\right]^3 \tag{5.18}$$

Here A_t^+ is the fully turbulent value and $Re_{\theta s}$ is the momentum-thickness Reynolds number at the start of transition (as determined by the correlation of Abu-Ghannam and Shaw [81]). The transitional value of A^+ only is used when $Re_{\theta s} < Re_\theta < 2Re_{\theta s}$. For the limited number of cases checked, the agreement is satisfactory.

Fujisawa, Rodi, and Schönung [46] modify the form of A^+ so that the empirical relation includes both the beginning and ending transition Reynolds numbers.

$$A^+ = A_t^+ + \left(300 - A_t^+\right)\left[1 - \sin\left(\frac{\pi}{2}\frac{Re_\theta - Re_{\theta s}}{Re_{\theta e} - Re_{\theta s}}\right)\right]^3 \tag{5.19}$$

where $Re_{\theta s}$ and $Re_{\theta e}$ are the Reynolds numbers associated with the start and end of transition (as determined by the Abu-Ghannam and Shaw [81] correlations). Fujisawa, Rodi, and Schönung [46] also use a different matching condition. The one- and two-equation models match where

$$y^+ = 6.1A^+\sqrt{\frac{u_\tau^2}{k}} \tag{5.20}$$

The computed results compare reasonably well with the results from several experiments, even with those from the strong acceleration case of Blair and Werle. [76] (See figure 3.) This particular result is surprising because A^+ is based on momentum thickness and the laminar momentum thickness decreases near the minimum Stanton number in the experiments. A careful review of this result reveals that, for this case, the good agreement is accidental; the Abu-Ghannam and Shaw correlation predicts the onset of transition upstream of the minimum Stanton number ($Re_\theta \approx 300$ from correlation;

$Re_\theta \approx 365$ at minimum Stanton number). This fortuitous occurrence initiates the turbulence model sufficiently far upstream where the momentum thickness is still increasing. Enough turbulence is generated that the momentum thickness never decreases. In some other case, the gods of transition and turbulence might not smile so brightly; this model has as much potential for failure as the ONERA/CERT model.

Rodi, Liu, and Schönung [48], and more recently Cho, Liu, Rodi, and Schönung [47], have adapted versions of the two-layer model for application to wake-induced unsteady flow by using the model in a Lagrangean way. Unsteady boundary conditions that correspond to the wake-perturbed flow field are used at the upstream end of the domain. Fluid elements near the boundary-layer edge are tracked and the local growth of Re_θ is monitored and compared with the theoretical Re_s for the pressure-gradient and free-stream turbulence parameters in that location at that time. When Re_θ first exceeds the local Re_s, that value of Re_s is frozen and used in the determination of A^+ for all downstream locations of that fluid element. With this model, the predicted flow quantities agree well with experiment over most of the surface. However, discrepancies occur with the turbulence intensities near the leading edge of the turbine blades because the boundary layer is quite thin in this area. This discrepancy at the leading edge does not result in problems further downstream.

5.3.2 Schmidt and Patankar $k-\epsilon$ Model

Based on the knowledge gained from their comparative study, Schmidt and Patankar [82] discuss a $k-\epsilon$ model that gives reasonably accurate indications of the starting point and extent of transition in a number of flows. Their modifications fit into the general scheme of low Reynolds number $k-\epsilon$ models and satisfy two additional requirements:

1. A well-defined region exists where starting profiles can be specified with minimal sensitivity.

2. The transition predictions determined starting and ending locations that agree well with the Abu-Ghannam and Shaw [81] correlations.

Schmidt and Patankar's [82] specific modifications are tailored to the Lam and Bremhorst [43] low Reynolds number form of the $k-\epsilon$ model. Instead of

modeling the turbulent kinetic-energy production term $P_k = \rho\overline{u_i' u_j'}\,(\partial \bar{u}_i/\partial x_j)$ with the standard eddy-viscosity approximation, Schmidt and Patankar [82] also constrain how fast the production term can grow and, consequently, the rate at which transition proceeds. Without understanding the detailed processes, they are able to meet their second objective with an empirical formulation where

$$\frac{dP_{k\max}}{dt} = B_1 P_k + B_2 \tag{5.21}$$

in which B_1 and B_2 are empirical parameters. They require that $P_k = 0$ where the momentum-thickness Reynolds number is below a critical value. Of course, the applicability of the model is limited to those cases for which their value of the critical momentum thickness is appropriate, although even with no production of k inside the boundary layer, kinetic energy can be convected into the boundary layer from the free stream. Schmidt and Patankar also modify the eddy-viscosity damping function f_μ so that it never exceeds unity (it never should). This change allows the $k-\epsilon$ model to simulate transition with free-stream turbulence levels less than 1%. The coefficients B_1 and B_2 are determined by numerical optimization over a wide range of turbulence intensities from 0.5% to 10%.

Schmidt and Patankar's [82] new model is insensitive to the starting location when the initial x-Reynolds number is less than 1000. For these initial starting locations, the solution is also insensitive to the starting profiles. The calculation results are compared with the results of 16 separate experiments that were performed by three different experimenters for a variety of free-stream turbulence levels and pressure gradients. For the high free-stream turbulence cases of Blair and Werle [76], Schmidt and Patankar [82] predicted transition somewhat earlier than actually occurred in the experiments. The model agrees much better with the data of Rued [83]. Satisfactory agreement is also obtained with the turbine-blade experiments of Daniels [84]. Because this model, like the Rodi models [31, 46, 48, 47], is triggered by an Re_θ condition, it can also fail if the laminar momentum thickness decreases before the turbulence model takes effect.

5.3.3 Wilcox $k-\omega$ Model

Wilcox [85] modified his $k-\omega$ model to account for low Reynolds number and transitional-flow effects. As with Schmidt and Patankar [79, 82], the

modifications delay the onset of transition and extend the length of the transition region. In Wilcox's model, the constants in the standard version of the $k-\omega$ model are functions of the turbulent Reynolds number $R_T = k/(\omega\nu)$. In the high Reynolds number version, $\alpha^* = 1$; the newer version uses

$$\alpha^* = \frac{\alpha_0^* + \frac{R_T}{R_k}}{1 + \frac{R_T}{R_k}} \tag{5.22}$$

with $\alpha_0^* = \beta/3$ and $R_k = 6$. As the turbulent Reynolds number gets large, α^* goes to its high Reynolds number value. Similarly, α, which was equal to 5/9, now goes asymptotically to that value; however, for lower turbulent Reynolds numbers, α is

$$\alpha = \frac{5}{9} \cdot \frac{1}{\alpha^*} \cdot \frac{\alpha_0 + \frac{R_T}{R_w}}{1 + \frac{R_T}{R_w}} \tag{5.23}$$

where $R_w = 2.7$. The constant β retains its value of 3/40 while

$$\beta^* = \frac{9}{100} \cdot \frac{\frac{5}{18} + \left(\frac{R_T}{R_\beta}\right)^4}{1 + \left(\frac{R_T}{R_\beta}\right)^4} \tag{5.24}$$

with $R_\beta = 8$. The three constants R_β, R_w, and R_k control the rate at which the closure coefficients approach their high Reynolds number values. Their values are the result of computer optimization and comparison with turbulent sublayer statistics. The model has been tested for transitional flow of an incompressible fluid over a flat plate. The starting locations of transition as a function of free-stream turbulence intensity agree reasonably well with the data of Dryden [86], although some sensitivity to the free-stream value of ω exists. The extent of the transition region as a function of the starting location of transition gives a satisfactory match with Dhawan and Narasimha's data [66]. The free-stream value of ω apparently does not affect the transition-region length.

5.3.4 LES Models for Transition

Piomelli and Zang [87] and Zang and Piomelli [88] tested several SGS models for LES of transitional flow. They found that the standard Smagorinsky type of model was overly dissipative, but that transitional phenomena

could be adequately captured using an intermittency function which varied as $(H_l - H)/(H_l - H_t)$. Here, H is the shape factor and the subscripts l and t refer the laminar and fully turbulent values, respectively. Another SGS model that is based on renormalization group theory was also used. The SGS stresses were essentially zero in the linear and early nonlinear stages of transition. The model captured most of the physical features of transition, but the quantitative results were very grid dependent. The formulation of the dynamic Smagorinsky SGS model by Germano et al. [62], which was described earlier was also used. This model, which allows for backscatter, gave the best predictions of mean-flow quantities of the transitional flow.

Quite recently, El-Hady, Zang, and Piomelli [89] performed LES calculations of a Mach 4.5 transitional boundary layer along a hollow cylinder using both the Germano et al. [62] and Lilly [64] formulations of the dynamic Smagorinsky SGS model. This work is ongoing, but preliminary results indicate that both formulations work well. Comparisons with the results of the direct numerical simulations performed by Pruett and Zang [90] on the same geometry indicate that the version of the dynamic Smagorinsky model suggested by Lilly [64] is somewhat more accurate than the original version by Germano et al. [62].

5.3.5 Questions Regarding Model Initiation

As noted earlier, linear-combination and algebraic models are sensitive to the choice of transition starting location. A similar problem arises with differential transition-region models, although, in this case, the problem involves the specification of initial turbulence profiles. In the past, variations in the starting locations and initial profiles for the turbulent statistics were not well documented. The same model could produce vastly different results for the same basic flow conditions; the differences were dependent upon the details of the initial conditions. Rodi and Scheuerer [45, 80] reduced the confusion by introducing initial profile functions that satisfied some basic constraints on k and ϵ. According to Rodi and Scheuerer [80], the profile for k vanishes at the wall, increases quadratically with distance from the wall, and asymptotes to the free-stream value. Their expression that meets this criteria is

$$k = k_e \left(\frac{U}{U_e} \right)^2 \tag{5.25}$$

Fewer constraints must be imposed on the ϵ profile. In the free stream, ϵ must go to its free-stream value; Rodi and Scheuerer [45, 80] argue that the length scale $k^{3/2}/\epsilon$ inside the boundary layer should not exceed the length scale in the free stream. They assume that the initial dissipation rate is proportional to the production rate of k so that

$$\epsilon = a_1 k \left(\frac{\partial U}{\partial y} \right) \qquad (\epsilon > \epsilon_e) \tag{5.26}$$

where a_1 is a function of the free-stream turbulence level. Rodi and Scheuerer's [45, 80] calculations start with $Re_\theta < 100$, where they claim that the flow is still stable and laminar. Schmidt and Patankar [79, 82] use similar profiles, although they take a_1 to be constant ($a_1 = 0.1$). Schmidt and Patankar [79, 82] also begin their calculations earlier; their results were insensitive to the initial profiles of k and ϵ when $Re_\theta \leq 25$. Abid [91] reports that predictions are independent of starting profiles for most $k - \epsilon$ models when $Re_x < 1000$. Abid [91] indicated that the Launder and Sharma model [42] had the more stringent starting requirement ($Re_x < 100$) in order to be independent of initial profiles. For flow over a flat plate, these Re_x values correspond to $Re_\theta = 21$ and $Re_\theta = 6.6$, respectively. In all studies that report different sensitivities, the results are more sensitive to the initial ϵ profiles than to the initial k profiles. Starting profiles for RST models have not been extensively explored; however, Savill [92] indicated that his results do not depend strongly on the normal stress distribution, but are sensitive to the assumed ϵ profile. The effects of starting conditions have not been explored with LES models. However, the sensitivity of the transition process to the initial disturbance field has been documented with DNS [93, 94]; hence this sensitivity will likely to be a problem for LES.

5.4 Unconventional Approaches

In this section, I will outline some novel ideas that have been proposed, but are not currently in vogue. Some of these ideas, for good reasons, will probably never be useful; others, with some work, could hold some promise in the future.

The renormalization group (RNG) theory of Yakhot and Orszag [95] suggested that many different levels of turbulence models, and even transition

models, could be obtained in a straightforward manner. Unfortunately, the algebraic RNG model for transition simulation that was studied by Lund [96] produced discontinuities in the turbulent eddy viscosity. Although the qualitative behavior of the model was correct, oscillations in the solutions cast doubts about the reliability of the model for flows more complex than flat-plate boundary layers. The RNG-based SGS model for LES performed somewhat better [97], largely because the model was inactive for much of the calculation. In more recent calculations, the results are very grid sensitive [88]. This bleak picture for RNG-based models may change in the future. Smith and Reynolds [98] found an algebraic error in the derivation of the skewness and identified several problems in the derivation of the energy-dissipation-rate equation. Future models with alternative derivations may prove more useful than their predecessors.

Young, Warren, Harris, and Hassan [99] modeled transition for the incompressible flow over a flat plate with low levels of free-stream turbulence. They explicitly included the effects of Tollmien-Schlichting (TS) waves by modifying the eddy-viscosity length scale. The new length scale incorporates TS wavelength information for a fraction $(1-\gamma)$ of the time. Unfortunately, in the true physical scenario, no true TS waves remain in the flow when $\gamma \neq 0$, although relics of their length scale may still exist. Young et al. also adjusted the equations to account for the large scales in the flow that were neither laminar nor turbulent. Both of these corrections had little effect on the shear stress, but had a large effect on the turbulent intensities.

Vancoillie and Dick [100] developed an incomplete model in which the effects of the intermittency of turbulent spots were incorporated directly into the k and ϵ equations. Conditional averaging was used so that the laminar and turbulent portions of the flow could be time-averaged (or ensemble-averaged) separately; the number of continuity and momentum equations to be solved was doubled, at least in the transitional-flow regime. Gradients of the intermittency appeared in the equations. Dhawan and Narasimha's [66] intermittency distribution was used, and the starting and ending locations of transition were assumed known. To date, this method has limited practical value. Vancoillie and Dick [100] computed boundary layers that corresponded to the experiments of Schubauer and Klebanoff [101], Juillen and Arnal [102], and Blair and Werle [76]. The results showed good agreement with experiment, particularly when the transition region was long when compared with the length of the boundary layer. Where the transition region was short, as

in the case of strong adverse pressure gradients, Vancoillie and Dick's [100] method did not perform well as it did for zero-pressure gradients.

Chapter 6

Evaluation of Transition Models

An appropriate transition model should be **easy to use**, computationally **inexpensive**, and **likely** to provide **accurate** results for all **conceivable** transitional flow situations. The degree of emphasis placed each of the words in bold-faced type is largely an individual choice. After these choices have been made, adequate information about the possible models must be obtained. The remainder of this chapter explores sources of information for selecting a model when the priorities have been established.

6.1 A Systematic Method

Singer and Dinavahi [75] proposed a strategy for testing transitional flow models. Because they were model users rather than developers, Singer and Dinavahi [75] avoided *a priori* biases regarding whether the models would run successfully. Rather, they identified the test problems and emphasized the procedure for handling diverse flow types with multiple examples. Specifically, they suggested

1. identify the major flow types for which the model will be used,
2. find appropriate experiments that illustrate the important physics, and
3. compare the model predictions with the experimental data.

For example, Singer and Dinavahi [75] considered the requirements for a transition-region model to calculate flows over high-speed aerodynamic vehicles. An **easy** and **inexpensive** algebraic turbulence model was used, which limited them to linear-combination and algebraic transition-region models. Singer and Dinavahi [75] selected a form of the Dey and Narasimha model [18] (linear-combination) and a model developed at ONERA/CERT [72, 73, 24] (algebraic).

They assumed that some other method could be used to determine the start of transition; the model needed to predict only the flow in the transition region. Seven types of transitional flows were identified that could **conceivably** be important for a high-speed aerodynamic vehicle. These test flows included two-dimensional incompressible constant-pressure boundary layers; boundary layers with pressure gradients; supersonic flows; flows with free-stream turbulence; flows with rough surfaces; flows with streamline curvature; and three-dimensional boundary layers. This list might seem extensive; however, it is by no means complete. A gas-turbine application would probably include transition in a boundary layer with mass injection and possibly transition in separation bubbles. A combustor application would require chemically reacting flows and free-shear layers. The list could continue; however, Singer and Dinavahi [75] emphasize the responsibility of the user to identify the relevant physical phenomena that will influence the transition process for the specific application.

In the next step, experiments that illustrated transition in the selected situations were chosen. Numerous criteria for the choice of experimental data were discussed. For example, some quantity that can be related to both the beginning and the end of transition must be measured. Ideally, measurements throughout the transition region were desired; however, the locations of the beginning and end of transition (determined by some well-defined criteria) were acceptable. Singer and Dinavahi [75] stressed simple geometries for two reasons: to minimize extraneous effects that might influence the transition process and to avoid the numerical difficulties associated with constructing complicated grids and solving the relevant equations on those grids. Finally, Singer and Dinavahi [75] noted that transition experiments are often sensitive to flow details that are not explicitly measured, such as very small scale surface roughness near the leading edge and the free-stream turbulence length scale and spectrum. The uncertainty in these quantities is typically not reflected in the experimental uncertainty of the measurements. Singer and

Dinavahi [75] also urged the use of multiple experiments for the same flow type, preferably performed in different facilities. The larger the data set, the less likely that overly general conclusions will be drawn. Unfortunately, they did not always follow their own advice; some flow types were not represented by a suitable diversity of experiments. This problem is being addressed with an extension to the database.

The models were used to predict the mean-flow in the test cases. When the intermittency was provided by the experimenters, an extrapolation of $\sqrt{-\log(1-\gamma)}$ to zero provided the point at which the models were initiated. When intermittency was not provided (the usual case), the models were initiated at a streamwise position that corresponded to 91% of the distance to the local minimum of some mean-flow property (e.g., skin-friction coefficient, Stanton number, surface pitot-tube pressure, etc.). The use of strict criteria for the starting positions of the models eliminated the subjective adjustments that many modelers have used to make their results correspond better. (For example, see reference [33], where the surface roughness was varied to better fit the data; reference [35], where free-stream turbulence levels were varied; and reference [103], where the starting location of transition was optimized on a case-by-case basis. Many other cases exist in which a similar optimization is suspected; the authors of the above references were careful enough to report what was done.)

A total of 24 test cases were run; the results were reported in reference [28] and were made available electronically to other modelers.

The extensive testing illustrated some important points.

1. The ONERA/CERT model can fail to predict any transition for a strong favorable-pressure-gradient case. (See fig. 3.) This failure to predict transition has been traced to the fact that the momentum thickness in the laminar boundary layer begins to decrease just before the model is initiated. Any model of the transition region that depends on an essentially monotonic increase of the momentum thickness through the transition zone (e.g., the transitional-flow correction to the two-layer model developed at Karlsruhe) is subject to this problem.

2. Linear-combination models cannot be used on flows for which the laminar flow would have separated, even if the transitional flow remains attached, because the laminar flow through the transition region is re-

quired to construct the appropriate linear combination.

3. The initiation of a turbulent boundary layer with zero boundary-layer thickness (as is required by linear-combination models) along a three-dimensional front that is not perpendicular to the streamlines is difficult. Without a clean method for performing this computation, linear-combination models in strongly three-dimensional flows are not practical.

4. Not surprisingly, the transitional-flow results depend on the turbulence model used.

5. Appropriate methods for initiating the transitional-flow model should be developed.

6. High levels of free-stream turbulence can influence the laminar flow before a transition-region model is initiated. This influence may not be a problem for models that solve a transport equation for the turbulence; however, algebraic and linear-combination models do not show any effect of the free-stream turbulence before transition begins.

After the testing was completed, Singer and Dinavahi [75] felt that a single transition-region model was not appropriate for all flows considered and suggested a "conglomerate model" that employs several submodels (or different coefficients for the same basic model). Each of these submodels would be optimized for a particular category of flows and selected by an experienced user (or perhaps an expert-system program).

6.2 The T3 Test-Case Project

The Europeon Research Community on Flow Turbulence and Combustion (ERCOFTAC) Special Interest Group (SIG) on transition and retransition has established a program for the assessment of turbulence models for engineering applications. The project is coordinated by Dr. A. M. Savill, a Rolls-Royce Senior Research Associate in the Engineering Department of the University of Cambridge in England. Savill outlines the program and summarizes the early results in reference [92]. More recent results have been reported in references [104] and [57].

Test cases T3A-, T3A, T3B, and T3C correspond to experiments performed at the Rolls Royce Applied Science Laboratory by Roach and Brierley [104, 105] to investigate the effects of isotropic free-stream turbulence on transition in zero-pressure-gradient boundary layers (cases T3A-, T3A, T3B) and in a favorable-to-adverse pressure-gradient boundary layer (case T3C). As additional experiments are performed, the number of test cases will be increased. (Unpublished data by Niew and Gaster of Cambridge University are being used to specify a case of transition following laminar separation [104].) Stow, Birch, Price, Roach, Brierley, and Cholerton of Rolls Royce (See reference [104].) prepare the specifications for the test cases. Typical test case specifications include velocity, turbulent kinetic energy, and dissipation-length-scale distributions in the free stream. The more recent experiments also include boundary-layer profiles of streamwise mean and perturbation velocities at a specified streamwise location on the flat plate. Suggested dissipation profiles are also provided. Participants in the program are requested to provide plots of the skin-friction coefficient C_f and the shape factor H against $\log Re_x$ and x.

The first report [92] includes 16 different sets of results, which were provided by nine research groups. No standard for numerical accuracy was imposed; each research group provided results that they felt were adequately resolved. In spite of the inclusion of a suggested Reynolds stress profile in the original specification, some investigators used a different profile instead of or in addition to the specified one. The conclusions indicate that the initial Reynolds stress profiles are not particularly important to the results; the results are more sensitive to the initial dissipation-rate profiles. Computation times were not always reported, but the available data suggest that these times varied from a few minutes on a VAX or IBM mainframe (typical of parabolic schemes) to hundreds of hours on a CRAY X-MP for a DNS. Only cases T3A and T3B were included in the initial report. Some highlights from the results are discussed below.

A DNS performed by Yang and Voke [106] closely matched the experimental data for skin friction and shape factor even though the grid resolution ($255 \times 32 \times 16$) was extremely coarse for a turbulence calculation. The LES performed by Mortenssen, Eriksson, and Albraten [107] using a standard Smagorinsky model without special transitional-flow treatment did not undergo transition. However, the recent dynamic-scale Smagorinsky models described in Section 5.3.4 were not tested for this flow; these models may

predict mean-flow properties as well as the DNS. Savill [108] used an RST model with various low Reynolds number closures. Only the Launder-Sharma low Reynolds number closure (see Section 4.3) underwent transition in both test cases; in both cases, this closure performed well. For two-equation models, those that used the Launder-Sharma low Reynolds number closure performed better than other models. Although this closure is asymptotically correct for ϵ and $\overline{u'v'}$ in turbulent flows, the fact that it depends primarily on $R_T = k^2/(\epsilon\nu)$ is probably more important because R_T does not depend directly on the the distance from the wall (unlike R_y or y^+). Other models that perform well in fully turbulent flow might do better for transitional flow if they were reformulated with R_T rather than R_y dependencies. The $k-\epsilon$ models were surprisingly insensitive to the initial k profile, but were very sensitive to the initial ϵ distributions. In most two-equation models, the skin-friction peak was not correctly predicted and the transition length was too short. Many of these observations were concurrently observed by Schmidt and Patankar [79]. Unfortunately, the Schmidt and Patankar model [82] was not included in the assessment program.

Subsequent reports of this program have included additional results from original contributors and new participants. The number of flow cases has also increased. The new T3C case with a favorable-to-adverse pressure gradient is certainly important to the gas-turbine industry, although from a modeling viewpoint an examination of separate favorable- and adverse-pressure-gradient cases may have been more enlightening.

The lack of strict deadlines in the program has allowed for continuous input from the participants. Unfortunately, this lack of deadlines also means that a complete, well-documented synthesis of the data is difficult to obtain. Similarly, case specifications can only be obtained from Dr. Savill or from the other participants. As some of these difficulties are overcome, this program promises to become a great source of information on the performance of various transition models, particularly in those flows that are relevant to the gas-turbine industry.

6.3 All Data Are NOT Equal–Some Notes on the Use of Experimental Data

Transitional-flow data have often presented the research community with paradoxes and apparent inconsistencies. Most of the time, the problem is not a glaring mistake, but a surprisingly strong influence by some flow quantity (usually not measured) on the flow. In this section, I discuss a personal experience with seemingly disparate data taken from a much acclaimed experiment.

The ONERA/CERT algebraic transition-region model was to be evaluated for supersonic flow over a cone in very low-disturbance environments. I selected eight cases from the flight experiments of Fisher and Dougherty [109]; four of these cases had edge Mach numbers from 1.44 to 1.47. For these four cases, I was interested in testing for strong unit Reynolds number effects in the flight experiments. Pate [110] illustrated strong unit Reynolds number effects in noisy wind tunnels and even in some ballistic-range data. Would these effects also be noticeable in flight tests? By luck, I found two cases from this group that had nearly identical unit Reynolds numbers. The predicted results for the two cases were essentially the same. The experimental results showed something different.

Detailed data from Flight 339 at time 13:13 and Flight 335 at 13:53 as reported in reference [109] are shown in table 6.1. The notation in the table is the same as that used in reference [109]; the nominal mean flow is characterized by the Mach number at the edge of the boundary layer M_e, the unit Reynolds number Re_1, the total temperature T_T, and the dynamic pressure q_∞. For all of these quantities, the differences between the two cases are less than 5%. The free-stream turbulence is described by the ratio of the root-mean-square total-pressure fluctuations $\sqrt{p_T'^2}$ to the dynamic pressure. Here, the difference between the two cases is about 7.5%. The pitch α and yaw β angles (in degrees) differ in the two cases. The two cases also differ in how closely the wall temperature approximated the adiabatic wall condition $T_w/T_{aw} = 1.0$. The Reynolds number at the start of transition Re_{t0} and the Reynolds number at the end of transition Re_{T0} correspond to the axial distance along the cone at which minimum and maximum surface pitot pressures were measured. The transition Reynolds numbers reported were already corrected (through empirical correlations) to account for the small

Flight	M_e	Re_1	T_T	T_w/T_{aw}	q_∞	$\sqrt{p_T'^2}/q_\infty$	α	β	Re_{t0}	Re_{T0}
339	1.44	11.04	317.3	1.023	34.14	2.30×10^{-4}	-0.07	-0.08	7.20	8.06
335	1.46	10.94	324.3	1.041	35.58	2.49×10^{-4}	-0.10	-0.07	7.57	9.23

Table 6.1: Two flight cases from Fisher and Dougherty [109]. The unit Reynolds number Re_1 is in units of $1/m$, the total temperature T_T is in degrees Kelvin, the dynamic pressure q_∞ is in units of KN/m^2, and the pitch α and yaw β angles are in degrees. All of the Reynolds numbers Re_1, Re_{t0}, and Re_{T0} have been multiplied by 10^{-6}.

deviations from adiabatic wall temperatures and nonzero incidence angles. Even without the corrections, the small differences measured in the two flight environments in no way suggest the difference of nearly a factor of 2 in the length of the transition region ($Re_{T0} - Re_{t0}$), particularly when both cases start transition at nearly the same Reynolds number. Which data point should be used to calibrate a model? Which should be used to report results? Singer, Dinavahi, and Zang [74] found that the ONERA/CERT model performed well for the second case and poorly for the first case. If the experiment did not measure (or did not report) one of these data points, how much faith can be put in the other point?

The Fisher and Dougherty flight experiments are considered high-quality work and remain an excellent source of data. With a traditional measure of transition-region length Re_{T0}/Re_{t0}, the ratios for the two cases are 1.12 and 1.22. The factor-of-2 difference in the length of the transition region does not appear so dramatic here, in particular because ratios from 1.1 to more than 2.0 have been found on the same cone in a variety of wind tunnels with the use of the same instrumentation and approximately the same Mach number (See figure 26 in reference [111].). The point is that a single case is not a sufficient basis for either model calibration or evaluation. Many more test cases are needed to assess the consistency of data and to determine the ability of the model to predict trends.

Chapter 7

Summary and Author's Views

This report began with experts' opinions of transitional-flow modeling. To understand modeling problems, various flow features that influence the transition process were discussed such as pressure gradients, compressibility, free-stream turbulence, surface roughness, streamline curvature, and mean-flow three-dimensionality. Various types of transition-region models were examined in table 3.1; rows of table 3.1 showed the level of modeling used for the turbulent flow and columns showed the level of modeling for the transition region. Different approaches to transition-region modeling require the use of different turbulence models. In later chapters some of the different models were explored in detail. The eddy-viscosity models involved the calculation of a turbulent eddy viscosity that is added to the molecular viscosity to calculate the mean flow. Determination of the eddy viscosity requires algebraic relationships or the solution of additional transport equations for various turbulence quantities (e.g., turbulent kinetic energy and turbulent length scale); these solutions are then combined to form an eddy viscosity. The RST models require the solution of separate equations for each of the turbulent stresses. In the LES approach, the SGS stresses must be modeled and the large-scale turbulent motions are computed. Modifications to these models to account for transitional flow often require additional empirical input. Finally, model assessment and the use of experimental data were discussed in the previous chapter. Throughout the text, I have tried to give a balanced view of the issues. The reader should now have sufficient knowledge to make his or her own judgments, so I will take this opportunity to offer my own opinions regarding transition-region models.

The simplest type of model that can simulate the mean-flow properties of a flow throughout the transition region for a reasonably large class of flows is LES. Only LES (after DNS) can track the temporal evolution of flow disturbances and preserves the frequency content of the free-stream disturbances, which is vital to the transitional process. No model that averages away this information truly simulates transition. Obviously, the LES approach is not a viable option for most scientists and engineers who need to know something about a particular transitional flow. What would I do in this case?

As rule of thumb, I restrict the level of transition-region model to no higher than needed to adequately describe the fully turbulent flow. The argument that higher order models include more physics of the flow and so should provide more reliable results is inappropriate for most transitional flows. Because transitional-flow physics is time-dependent, Reynolds averaging can smear the critical aspects of the physics. The only situations in which the transitional flow results may be improved (more than the fully turbulent results) by the use of higher order models are those that have high levels of free-stream turbulence because the free-stream turbulence can influence the laminar flow. In these cases, algebraic turbulence models might do well in the fully turbulent regime; however, a model that transports the turbulence into the boundary layer can improve the results for the nominally laminar flow before transition begins in earnest.

Turbulence models that are specifically modified to handle transitional flows can provide better results than models without any modification. Simply rewriting low Reynolds number closures in terms of R_T instead of R_y or y^+ is unlikely to produce high quality models for transitional flows. This approach might work well in many cases; however, it also will not work well in many cases. No guidelines exist to help the user distinguish between these cases *a priori*. I prefer to use models that have been closed with empirical information from transitional flows similar to those that will be computed. A variety of different closures, based on experiments for different kinds of transitional flow (similar to the conglomerate model mentioned in reference [75]), can be used wisely to great benefit. If a flow must be computed for which no relevant experimental information exists, then much larger errors should be expected.

Perhaps the most important lesson is never to believe a transitional flow prediction simply because it came out of a computer. If the answers do not conform with notions of how similar flows behave, then question what went

into the calculation and examine the expected accuracy of the result. I hope that this work has provided the necessary knowledge to facilitate the asking of the right questions.

Acknowledgments

Financial support for this work was provided by the Theoretical Flow Physics Branch, Fluid Mechanics Division, NASA Langley Research Center under contract NAS1-19299. The author would like to thank the following researchers for their input: Dr. Ridha Abid, Dr. Surya Dinavahi, Dr. Roger Grundmann, Christopher Kennedy, Prof. Brian Launder, Prof. Wolfgang Rodi, Dr. Mark Savill, Dr. Georg Scheuerer, Dr. Charles Speziale, Dr. Craig Streett, Dr. David Wilcox, Dr. Bassam Younis, and Dr. Thomas Zang.

Bibliography

[1] R. E. Mayle. The role of laminar-turbulent transition in gas turbine engines. *Journal of Turbomachinery*, 113:509–537, October 1991.

[2] R. Narasimha, K. J. Devasia, G. Gururani, and M. A. Badri Narayanan. Transitional intermittency in boundary layers subjected to pressure gradient. *Experiments in Fluids*, 2:171–176, 1984.

[3] R. Narasimha, C. Subramanian, and M. A. Badri Narayanan. Turbulent spot growth in favorable pressure gradients. *AIAA Journal*, 22(6):837–839, 1984.

[4] G. J. Walker and J. P. Gostelow. Effects of adverse pressure gradients on the nature and length of boundary layer transition. Paper No. 89-GT-274, ASME, 1989.

[5] S. Sarkar and B. Lakshmanan. Application of a Reynolds stress turbulence model to the compressible shear layer. *AIAA Journal*, 29(5):743–749, May 1991.

[6] S. R. Pate. Effects of wind tunnel disturbances on boundary-layer transition with emphasis on radiated noise: a review. Paper No. 80-0431, AIAA, 1980.

[7] D. M. Bushnell. Notes on initial disturbance fields for the transition problem. NASP TM 1051, NASA, March 1989.

[8] M. V. Morkovin. Bypass-transition research: issues and philosophy. In D. Ashpis, T. B. Gatski and R. Hirsh, editors, *Instabilities and Turbulence in Engineering Flows*. Kluwer Academic Publishers, 1993.

[9] I. Tani and Y. Aihara. Görtler vortices and boundary-layer transition. *ZAMP*, 20:609–618, 1969.

[10] H. L. Reed and W. S. Saric. Stability of three-dimensional boundary layers. *Annual Review of Fluid Mechanics*, 21:235–284, 1989.

[11] L. Mack. Boundary-layer linear stability theory. In *Special Course on Stability and Transition of Laminar Flow*. AGARD, 1984. Report No. 709.

[12] J. A. Masad and A. H. Nayfeh. Laminar flow control of subsonic boundary layers by suction and heat-transfer strips. *The Physics of Fluids A*, 4(6):1259–1272, June 1992.

[13] L. M. Mack. Review of linear compressible stability theory. In D. Dwoyer and M. Y. Hussaini, editors, *Stability of Temporal and Spatially Varying Flows*, pages 164–187. Springer, 1986.

[14] K. Rued and S. Wittig. Free-stream turbulence and pressure gradient effects on heat transfer and boundary layer development on highly cooled surfaces. *Journal of Engineering for Gas Turbines and Power*, 107:54–59, January 1985.

[15] J. N. Hefner. Dragging down fuel costs. *Aerospace America*, pages 14–16, January 1988.

[16] H. L. Reed and A. H. Nayfeh. Numerical-perturbation technique for stability of flat-plate boundary layers with suction. *AIAA Journal*, 24(2):208–214, February 1986.

[17] G. A. Reynolds and W. S. Saric. Experiments on the stability of the flat-plate boundary layer with suction. *AIAA Journal*, 24(2):202–207, February 1986.

[18] J. Dey and R. Narasimha. An integral method for the calculation of 2D transitional boundary layers. Report 88 FM 7, Department of Aerospace Engineering, Indian Institute of Science, Bangalore, India, 1988.

[19] O. Reynolds. On the dynamical theory of incompressible viscous fluids and the determination of the criterion. *Phil. Trans. Roy. Soc. A*, 186:123–164, 1895.

[20] S. J. Kline, D. J. Cockrell, M. V. Morkovin, and G. Sovran, editors. *Proceedings Computation of Turbulent Boundary Layers*, volume 1. Stanford University Mechanical Engineering Dept., 1968.

[21] D. E. Coles and E. A. Hirst, editors. *Proceedings Computation of Turbulent Boundary Layers*, volume 2. Stanford University Mechanical Engineering Dept., 1968.

[22] F. M. White. *Viscous Fluid Flow.* McGraw-Hill, 1974.

[23] J. E. Harris. Numerical solutions of equations for compressible laminar, transitional, and turbulent boundary layers, and comparisons with experimental data. Technical Report R–368, N 71–32164, NASA, 1971.

[24] D. Arnal. Laminar-turbulent transition problems in supersonic and hypersonic flows. In *Special Course on Aerothermodynamics of Hypersonic Vehicles.* AGARD, 1988. 30 May – 3 June.

[25] J. O. Hinze. *Turbulence.* Mc-Graw-Hill Book Company, 2nd edition, 1975.

[26] T. Cebeci and A. M. O. Smith. *Analysis of Turbulent Boundary Layers*, Volume 15. Academic Press, 1974.

[27] B. S. Baldwin and H. Lomax. Thin layer approximation and algebraic model for separated turbulent flows. Paper No. 78-257, AIAA, January 1978.

[28] B. A. Singer, S. P. G. Dinavahi, and V. Iyer. Testing of transition-region models: Test cases and data. CR 4371, NASA, May 1991.

[29] L. H. Norris and W. C. Reynolds. Turbulent channel flow with a moving wavy boundary. FM 10, Stanford Univ., Dept of Mech. Eng., 1975.

[30] W. Rodi. Some current approaches in turbulence modeling. Advisory Report 291, AGARD, 1990.

[31] W. Rodi. Experience with two-layer models combining the $k-\epsilon$ model with a one-equation model near the wall. Paper No. 91-0216, AIAA, January 1991. Presented at the 29th Aerospace Sciences Meeting, Reno.

[32] W. Rodi and G. Scheuerer. Scrutinizing the $k-\epsilon$ model under adverse pressure gradient conditions. *Journal of Fluids Engineering*, 108:174–179, 1986.

[33] H. Mc Donald and R. W. Fish. Practical calculations of transitional boundary layers. AGARDograph 164, 1972.

[34] H. McDonald and F. J. Camarata. An extended mixing length approach for computing the turbulent boundary layer development. In S. J. Kline, D. J. Cockrell, M. V. Morkovin, and G. Sovran, editors, *Proceedings Computation of Turbulent Boundary Layers*, volume 1, 1968.

[35] S. Shamroth and H. Mc Donald. Assessment of a transitional boundary layer theory at low hypersonic Mach numbers. CR 2131, NASA, 1972.

[36] G. Mavrantonakis and R. Grundmann. Transition in 3-D boundary layers with a one-equation model. In *Boundary Layer Transition and Control Conference*, pages 28.1–28.14. Royal Aeronautical Soc., 1991. 8–12 April, Cambridge, U.K.

[37] H. Deyhle and R. Grundmann. Transition model for prediction and calculation of boundary layers. *Z. Flugwiss. Weltraumforsch.*, 15:119–128, 1991.

[38] C. G. Speziale, R. Abid, and E. C. Anderson. Critical evaluation of two-equation models for near-wall turbulence. *AIAA Journal*, 30(2), February 1992.

[39] C. G. Speziale. Analytical methods for the development of Reynolds-stress closures in turbulence. *Annual Review of Fluid Mechanics*, 23:107–157, 1991.

[40] B. E. Launder and D. B. Spalding. The numerical computation of turbulent flows. *Computer Methods in Applied Mechanics and Engineering*, 3:269–289, 1974.

[41] W. P. Jones and B. E. Launder. The calculation of low-Reynolds-number phenomena with a two-equation model of turbulence. *Int. J. Heat Mass Transfer*, 16:1119–1130, 1973.

[42] B. E. Launder and B. I. Sharma. Application of the energy-dissipation model of turbulence to the calculation of flow near a spinning disc. *Letters in Heat and Mass Transfer*, 1:131–139, 1974.

[43] C. K. G. Lam and K. Bremhorst. A modified form of the $k - \epsilon$ model for predicting wall turbulence. *Journal of Fluids Engineering*, 103:456–460, 1981.

[44] V. C. Patel, W. Rodi, and G. Scheuerer. Turbulence models for near-wall and low Reynolds number flows: a review. *AIAA Journal*, 23(9):1308–1318, 1984.

[45] W. Rodi and G. Scheuerer. Calculation of heat transfer to convection-cooled gas turbine blades. *Journal of Engineering for Gas Turbines and Power*, 107:620–627, July 1985.

[46] N. Fujisawa, W. Rodi, and B. Schönung. Calculation of transitional boundary layers with a two-layer model of turbulence. In J. H. Kim and W.-J. Yang, editors, *Rotating Machinery: Transport Phenomena*, pages 651–663. Hemisphere Publishing Corporation, 1992.

[47] N.-H. Cho, X. Liu, W. Rodi, and B. Schönung. Calculation of wake-induced unsteady flow in a turbine cascade. ASME, June 1992. Presented at the Turbomachinery Expo, Cologne.

[48] W. Rodi, X. Liu, and B. Schönung. Transitional boundary layers with wake-induced unsteadiness. June 1989. Presented at the 4th Symp. on Numerical and Physical Aspects of Aerodynamic Flows, Long Beach, California.

[49] D. C. Wilcox. A half century historical review of the $k-\omega$ model. Paper No. 91-0615, AIAA, January 1991. Presented at the 29th Aerospace Sciences Meeting, Reno.

[50] D. C. Wilcox. Reassessment of the scale determining equation for advanced turbulence models. *AIAA Journal*, 26(11), November 1988.

[51] S. Hassid and M. Poreh. A turbulent energy dissipation model for flows with drag reduction. *Journal of Fluids Engineering*, 100, 1978.

[52] G. H. Hoffman. Improved form of the low-Reynolds number $k - \epsilon$ turbulence model. *The Physics of Fluids*, 18, 1975.

[53] D. Dutoya and P. Michard. A program for calculating boundary layers and heat transfer along compressor and turbine blades. In R. W. Lewis, K. Morgan, and O. C. Zienkiewicz, editors, *Numerical Methods in Heat Transfer*, pages 413–429. John Wiley and Sons Ltd., 1981.

[54] W. C. Reynolds. Computation of turbulent flows. *Annual Review of Fluid Mechanics*, 8:183–208, 1976.

[55] K.-Y. Chien. Predictions of channel and boundary-layer flows with a low-Reynolds-number turbulence model. *AIAA Journal*, 20(1), January 1982.

[56] D. C. Wilcox and M. W. Rubesin. Progress in turbulence modeling for complex flow fields including effects of compressibility. TP 1571, NASA, 1980.

[57] A. M. Savill. Turbulence model predictions for transition under free-stream turbulence. Poster paper, Royal Aeronautical Soc., 1991. RAeS Transition and Boundary Layer Conference, 8–12 April, Cambridge, U.K.

[58] W. Kebede, B. E. Launder, and B. A. Younis. Large-amplitude periodic pipe flow: a second-moment closure study. In *Proceedings of the Fifth Symposium on Turbulent Shear Flows*, pages 16.23–16.29, 1985. Cornell, 7–9 August.

[59] B. E. Launder and N. Shima. Second-moment closure for the near-wall sublayer: development and application. *AIAA Journal*, 27(10):1319–1325, 1989.

[60] J. Smagorinsky. General circulation experiments with the primitive equations. I. The basic experiment. *Monthly Weather Review*, 91, 1963.

[61] U. Piomelli, W. H. Cabot, P. Moin, and S. Lee. Subgrid-scale backscatter in turbulent and transitional flows. *The Physics of Fluids A*, 3(7):1766–1771, July 1991.

[62] M. Germano, U. Piomelli, P. Moin, and W. H. Cabot. A dynamic subgrid-scale eddy viscosity model. *The Physics of Fluids A*, 3(7):1760–1765, July 1991.

[63] P. Moin, K. Squires, W. H. Cabot, and Sangsan Lee. A dynamic subgrid-scale model for compressible turbulence and scalar transport. *The Physics of Fluids A*, 3(11):2746–2757, November 1991.

[64] D. K. Lilly. Analysis and extensions of the Germano subgrid-scale closure method. *The Physics of Fluids A*, 4(3):633-635, 1992. in press.

[65] H. W. Emmons. The laminar-turbulent transition in a boundary layer–Part I. *J. Aero. Sci.*, 18:490–498, 1951.

[66] S. Dhawan and R. Narasimha. Some properties of boundary layer flow during the transition from laminar to turbulent motion. *Journal of Fluid Mechanics*, 3, 1958.

[67] K. K. Chen and N. A. Thyson. Extension of Emmons' spot theory to flows on blunt bodies. *AIAA Journal*, 9, 1971.

[68] R. Narasimha. The laminar-turbulent transition zone in the boundary layer. *Prog. Aerospace Sci.*, 22:29–80, 1985.

[69] R. Narasimha. Subtransitions in the transition zone. In V.V. Kozlov, editor, *Laminar-Turbulent Transition*. Springer-Verlag, 1985.

[70] J. Dey and R. Narasimha. Effect of favorable pressure gradient on transitional spot formation rate. *Experimental Thermal and Fluid Science*, 4:192–197, 1991.

[71] J. Dey and R. Narasimha. Integral method for the calculation of incompressible two-dimensional transitional boundary layers. *J. Aircraft*, 27(10):859–865, 1990.

[72] D. Arnal. Description and prediction of transition in two-dimensional incompressible flow. In *Special Course on Stability and Transition of Laminar Flow*. AGARD, 1984. Report No. 709.

[73] D. Arnal. Three-dimensional boundary layers: laminar-turbulent transition. In *Special Course on Calcul Des Limites Tridimensionnelles Avec Ou Sans Decollement*. AGARD, 1986. 14-18 April.

[74] B. A. Singer, S. Dinavahi, and T. A. Zang. Evaluation of a compressible transition model. NASP CR 1109, NASA, January 1991.

[75] B. A. Singer and S. P. G. Dinavahi. Testing of transition-region models. *Journal of Fluids Engineering*, 114:73–79, March 1992.

[76] M. F. Blair and M. J. Werle. Combined influence of free-stream turbulence and favorable pressure gradients on boundary layer transition and heat transfer. Rept. R81-914388-17, United Technologies, 1981.

[77] C. DuP. Donaldson. A computer study of an analytical model of boundary-layer transition. *AIAA Journal*, 7(2), 1969.

[78] C. H. Pridden. *The Behavior of Turbulent Boundary Layer on Curved Porous Walls*. PhD thesis, Imperial College, London, 1975.

[79] R. C. Schmidt and S. V. Patankar. Simulating boundary layer transition with low-Reynolds-number $k - \epsilon$ turbulence models: Part 1–an evaluation of prediction characteristics. *Journal of Turbomachinery*, 113:10–17, January 1991.

[80] W. Rodi and G. Scheuerer. Calculation of laminar-turbulent boundary layer transition on turbine blades. Conference proceedings no. 390, AGARD, May 1985. Presented at the Propulsion and Energetics Panel 65th Symposium held in Bergen, Norway.

[81] B. J. Abu-Ghannam and R. Shaw. Natural transition of boundary layers–the effects of turbulence pressure gradient, and flow history. *J. Mech. Eng. Science*, 22(5):213–228, 1980.

[82] R. C. Schmidt and S. V. Patankar. Simulating boundary layer transition with low-Reynolds-number $k - \epsilon$ turbulence models: Part 2–an

approach to improving the predictions. *Journal of Turbomachinery*, 113:18–26, January 1991.

[83] K. Rued. *Transitionale Grezschichten unter dem Einflus hoher Freistromturbulenze, intensiver Wandkuehlung und starken Druckgradienten in Heissgasstroemungen.* PhD thesis, Univ. of Karlsruhe, 1983. (English Translation, NASA Rept. No. TM-88524, 1987).

[84] L. D. Daniels. *Film Cooling of Gas Turbine Blades.* PhD thesis, Dept. of Eng. Science, Univ. of Oxford, 1978.

[85] D. C. Wilcox. The remarkable ability of turbulence model equations to describe transition. In *Fifth Symposium on Numerical and Physical Aspects of Aerodynamic Flows*, 1992. 13-15 January.

[86] H. L. Dryden. *Aerodynamics and Jet Propulsion*, volume V. University Press, 1959.

[87] U. Piomelli and T. A. Zang. Large-eddy simulation of transitional channel flow. *Computer Phys. Comm.*, 65, 1991.

[88] T. A. Zang and U.Piomelli. Large-eddy simulation of transitional flow. In B. Galperin and S. A. Orszag, editors, *Large Eddy Simulation of Complex Engineering and Geophysical Flows.* Cambridge Univ. Press, 1992.

[89] N. M. El-Hady, T. A. Zang, and U. Piomelli. Dynamic subgrid-scale modeling for high-speed transitional boundary layers. To be presented at ASME FED Symposium on Engineering Applications of Large-Eddy Simulations, in Washington D. C. in June 1993.

[90] C.D. Pruett and T.A. Zang. Direct numerical simulation of laminar breakdown in high-speed axisymmetric boundary layers. *Theoretical and Computational Fluid Dynamics*, 3(6), 1992.

[91] R. Abid. Evaluation of two-equation turbulence models for predicting transitional flows. *Int. J. of Engr. Science*, in press 1993.

[92] A. M. Savill. A synthesis of T3 test case predictions. In *Proceedings of the 1st ERCOFTAC Workshop on Numerical Simulation of Unsteady*

Flows, Transition to Turbulence and Combustion. C. U. P., 1991. Lausanne.

[93] B. A. Singer, H. L. Reed, and J. H. Ferziger. The effects of streamwise vortices on transition in the plane channel. *Physics of Fluids, A*, 1(12):1960–1971, December 1989.

[94] U. Konzelmann, U. Rist, and H. Fasel. Numerical investigation of the effects of longitudinal vortices on the onset of transition in the flat plate boundary layer. Technical report, AGARD/FDP Symposium, October 1988. Presented at the Fluid Dynamics of 3D Turbulent Shear Flows Symposium held in Cesme, Turkey.

[95] A. Yakhot and S. A. Orszag. Renormalization group analysis of turbulence. i. basic theory. *J. Sci. Computing*, 1(1):3–51, 1986.

[96] T. S. Lund. Application of the algebraic RNG model for transition simulation. In M. Hussaini and R. Voigt, editors, *Instability and Transition (ICASE/NASA)*, pages 463–479. Springer, 1990.

[97] U. Piomelli, T. A. Zang, C. G. Speziale, and T. S. Lund. Application of renormalization group theory to the large-eddy simulation of transitional boundary layers. In M. Hussaini and R. Voigt, editors, *Instability and Transition (ICASE/NASA)*, pages 480–496. Springer, 1990.

[98] L. M. Smith and W. C. Reynolds. On the Yakhot-Orszag renormalization group method for deriving turbulence statistics and models. *The Physics of Fluids A*, 4(2):364–390, February 1992.

[99] T. W. Young, E. S. Warren, J. E. Harris, and H. A. Hassan. A new approach for the calculation of transitional flows. Paper No. 92-2669, AIAA, 1992.

[100] G. Vancoillie and E. Dick. A turbulence model for the numerical simulation of the transition zone in a boundary layer. *Journal of Engineering Fluid Mechanics*, pages 28–49, 1988.

[101] G. B. Scuhbauer and P. S. Klebanoff. Contributions on the mechanics of boundary-layer transition. TN 3489, NASA, 1955.

[102] J. C. Juillen and D. Arnal. Profils de vitesse moyenne et de turbulence mesurés das une couche limite de transition, en gradient de pression nul et positif. Rapport Technique OA 17/5018 AND, ONERA-CERT, 1981.

[103] S. Dinavahi. Comparison of two transition models. In M. Hussaini and R. Voigt, editors, *Instability and Transition (ICASE/NASA)*, pages 453–462. Springer, 1990.

[104] A. M. Savill. Predicting transition induced by free-stream turbulence. Technical report, IAHR/ERCOFTAC, 1992. Presented at J.M. Burgers Centre Dutch ERCOFTAC Pilot Centre, 29 June 1992.

[105] P. E. Roach and D. H. Brierly. The influence of a turbulent free-stream on zero pressure gradient transitional boundary layer development, including the T3A and T3B test case conditions. In *Proceedings of the 1st ERCOFTAC Workshop on Numerical Simulation of Unsteady Flows, Transition to Turbulence and Combustion*. C. U. P., 1991. Lausanne.

[106] Z. Y. Yang and P. R. Voke. Numerical simulation of boundary layer transition in the presence of free-stream turbulence. In *Proceedings of the 1st ERCOFTAC Workshop on Numerical Simulation of Unsteady Flows, Transition to Turbulence and Combustion*. C. U. P., 1991. Lausanne.

[107] H. E. Mortenssen, L. E. Eriksson, and P. J. Albraten. Contribution to the ERCOFTAC workshop at EPFL, March 26-28, 1990 flat plate transition test case T3. In *Proceedings of the 1st ERCOFTAC Workshop on Numerical Simulation of Unsteady Flows, Transition to Turbulence and Combustion*. C. U. P., 1991. Lausanne.

[108] A. M. Savill. Application of a low-Reynolds number Reynolds stress transport model to the prediction of transition under the influence of free-stream turbulence. In *Proceedings of the 1st ERCOFTAC Workshop on Numerical Simulation of Unsteady Flows, Transition to Turbulence and Combustion*. C. U. P., 1991. Lausanne.

[109] D. F. Fisher and N. S. Dougherty. Transition measurements on a 10^o cone at Mach numbers from 0.5 to 2.0. TP 1971, NASA, June 1982.

[110] S. R. Pate. Dominance of noise on boundary layer transition in conventional wind tunnels – a place for the quiet ballistic range in future studies. In M. Hussaini and R. Voigt, editors, *Instability and Transition (ICASE/NASA)*, pages 77–87. Springer, 1990.

[111] D. F. Fisher and N. S. Dougherty. Flight and wind-tunnel correlation of boundary-layer transition on the AEDC transition cone. AGARD CP 339 Paper No. 5, AGARD Flight Mechanics Panel Symposium, October 1982.

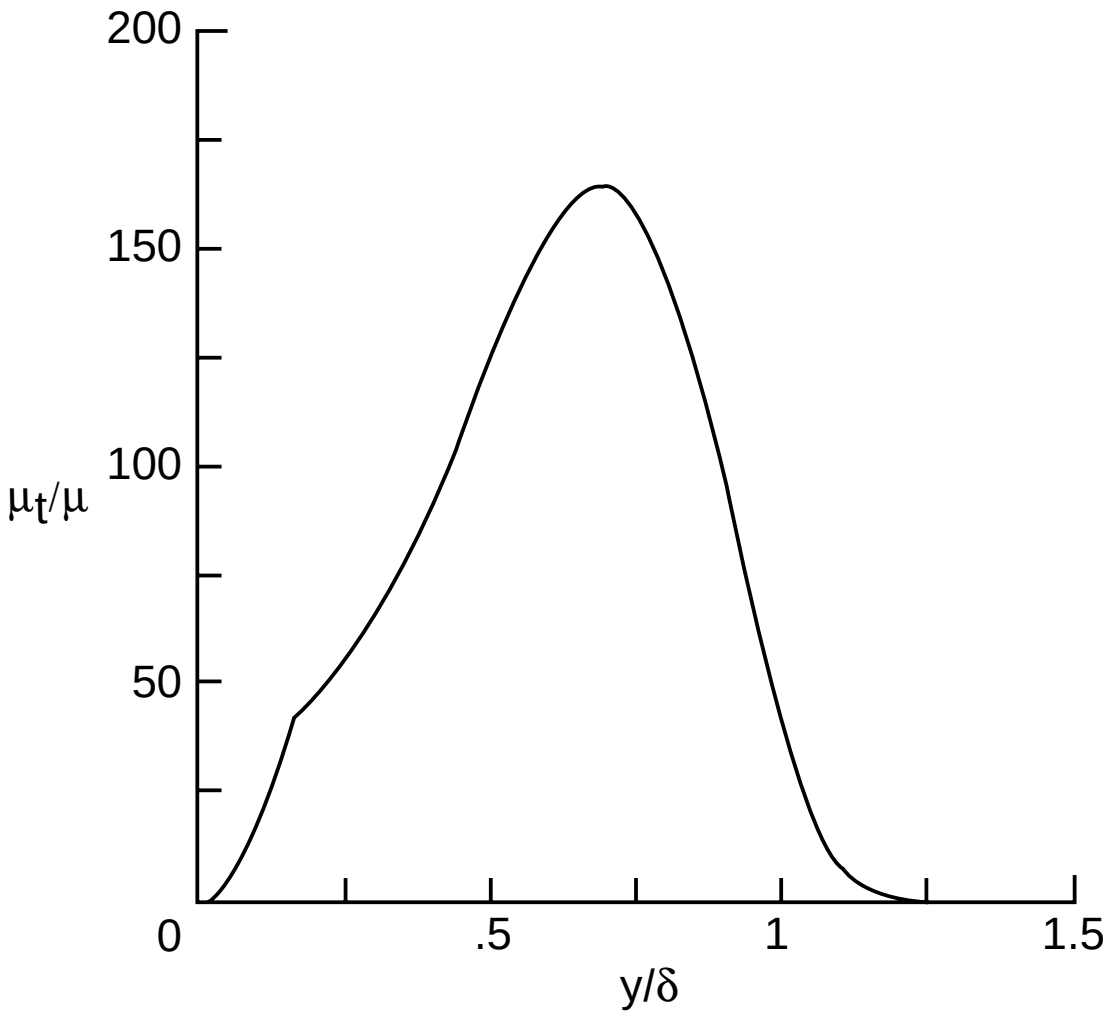

Figure 1: Typical profile of turbulent eddy viscosity through boundary layer.

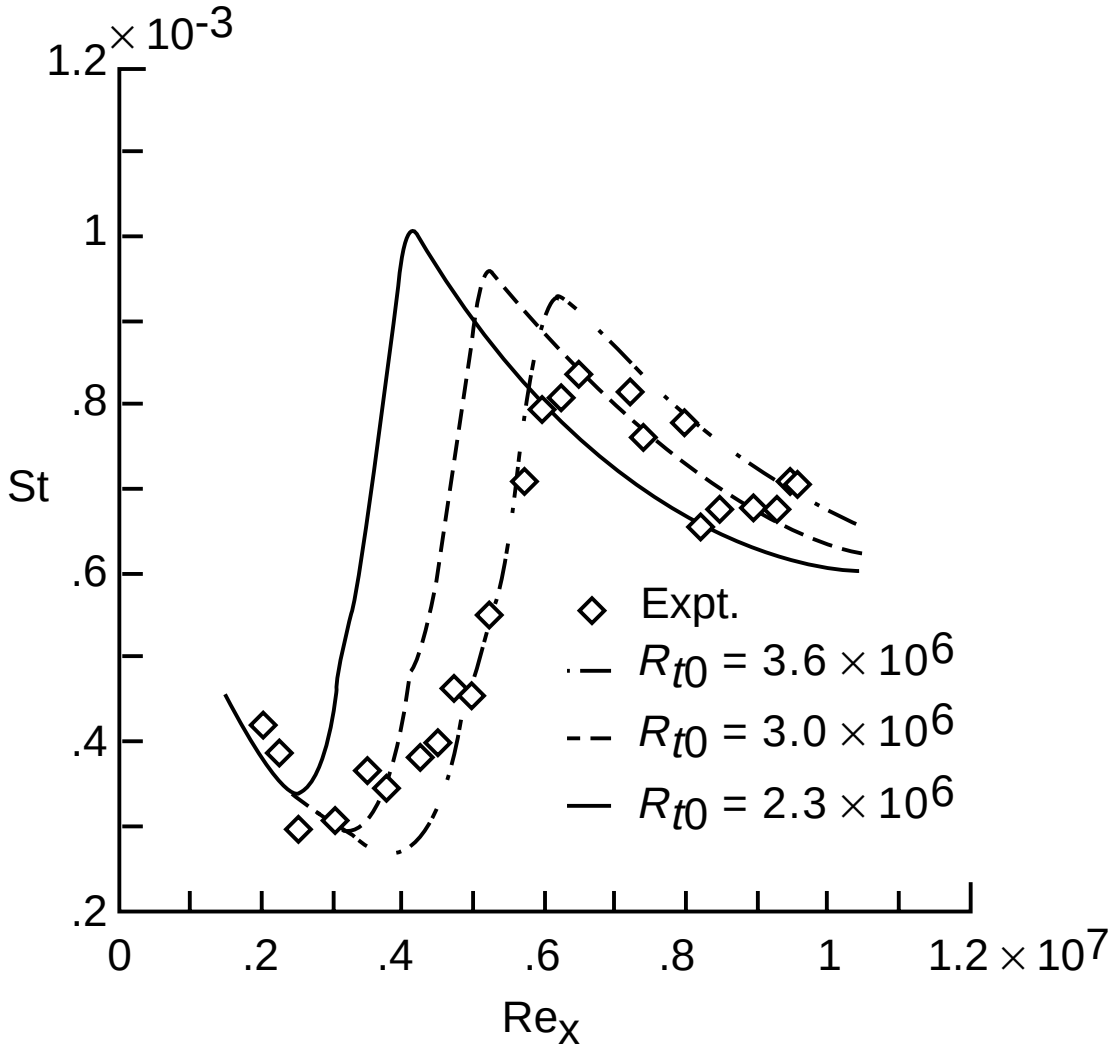

Figure 2: Streamwise variation of Stanton number for cold cone in Mach 8 flow. The ONERA/CERT model was used with different starting positions. Experimental data from Kimmel (personal communications).

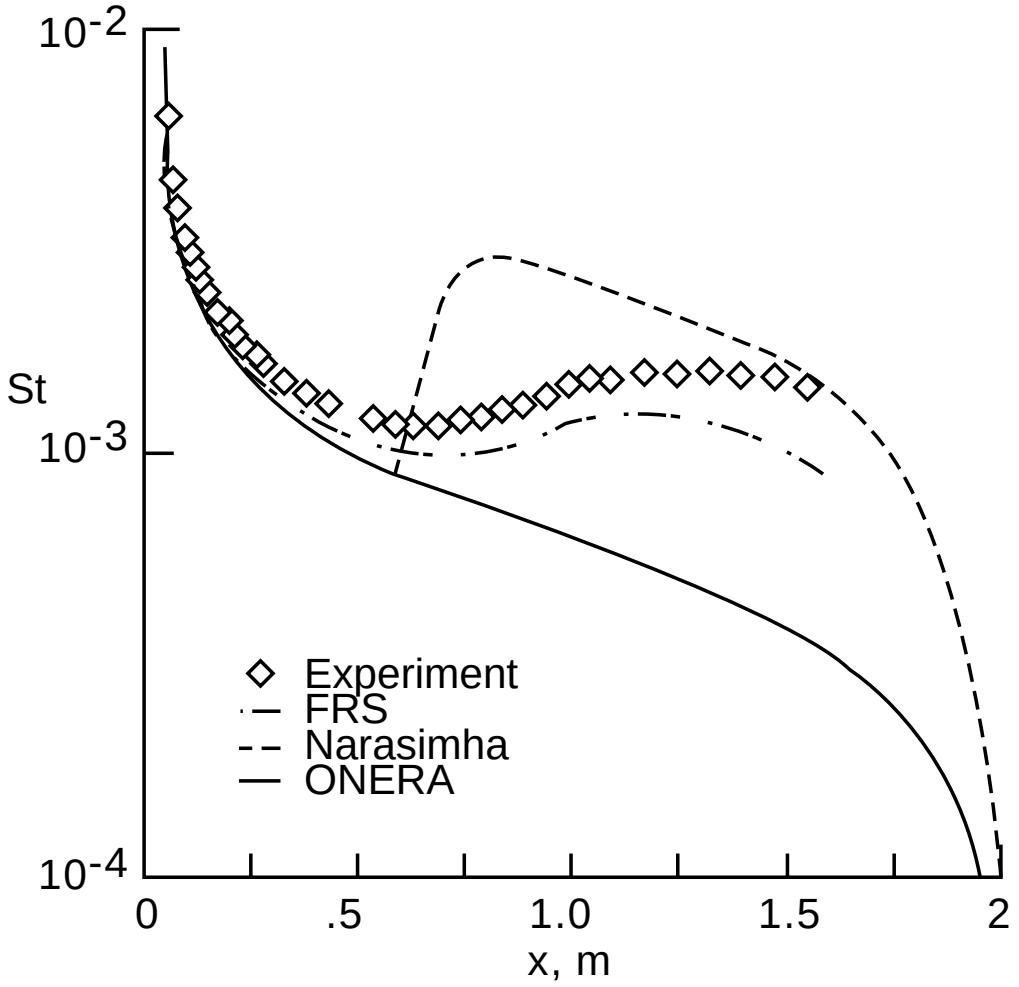

Figure 3: Streamwise variation of Stanton number for heated plate in strong favorable pressure gradient. Experimental data from Blair and Werle [76].

REPORT DOCUMENTATION PAGE

Form Approved
OMB No. 0704-0188

1. AGENCY USE ONLY *(Leave blank)*	2. REPORT DATE	3. REPORT TYPE AND DATES COVERED
	February 1993	Contractor Report

4. TITLE AND SUBTITLE
Modeling the Transition Region

5. FUNDING NUMBERS
NAS1-18240

6. AUTHOR(S)
Bart A. Singer

7. PERFORMING ORGANIZATION NAME(S) AND ADDRESS(ES)
High Technology Corporation
28 Research Drive
Hampton, VA 23666

8. PERFORMING ORGANIZATION REPORT NUMBER

9. SPONSORING/MONITORING AGENCY NAME(S) AND ADDRESS(ES)
National Aeronautics and Space Administration
Langley Research Center
Hampton, VA 23665-5225

10. SPONSORING/MONITORING AGENCY REPORT NUMBER
NASA CR-4492

11. SUPPLEMENTARY NOTES
Langley Technical Monitor: Craig L. Street

12a. DISTRIBUTION/AVAILABILITY STATEMENT
Unclassified–Unlimited

Subject Category 02

12b. DISTRIBUTION CODE

13. ABSTRACT *(Maximum 200 words)*

The current status of transition-region models is reviewed in this report. To understand modeling problems, various flow features that influence the transition process are discussed first. Then an overview of the different approaches to transition-region modeling is given. This followed by a detailed discussion of turbulence models and the specific modifications that are needed to predict flows undergoing laminar-turbulent transition. Methods for determining the usefulness of the models are presented, and an outlook for the future of transition-region modeling is suggested.

14. SUBJECT TERMS
transition; transition region; transition modeling; turbulence modeling

15. NUMBER OF PAGES
88

16. PRICE CODE
AO5

17. SECURITY CLASSIFICATION OF REPORT	18. SECURITY CLASSIFICATION OF THIS PAGE	19. SECURITY CLASSIFICATION OF ABSTRACT	20. LIMITATION OF ABSTRACT
Unclassified	Unclassified	Unclassified	